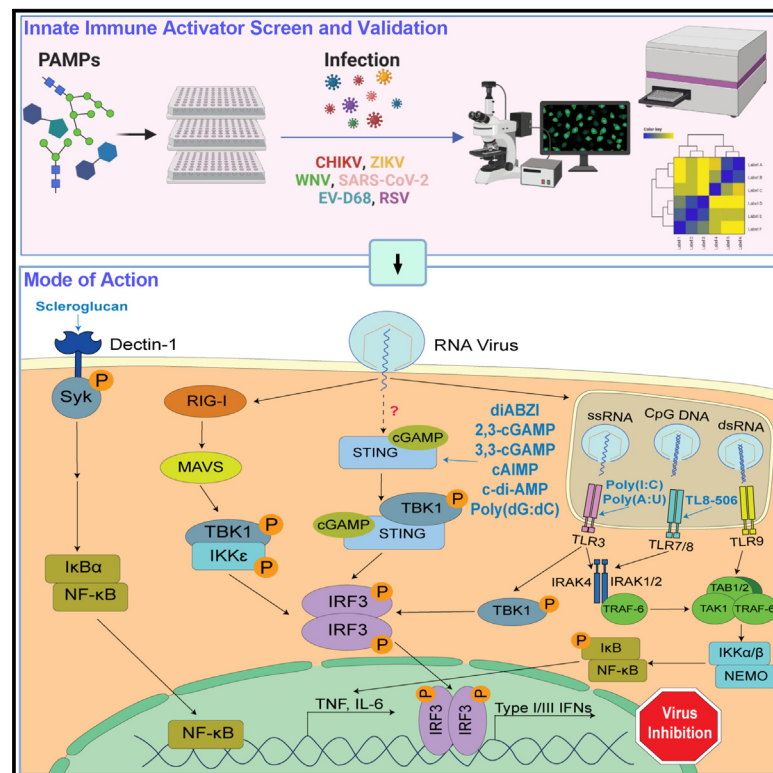


Innate immune pathway modulator screen identifies STING pathway activation as a strategy to inhibit multiple families of arbo and respiratory viruses

Graphical abstract



Authors

Gustavo Garcia, Jr.,
Joseph Ignatius Irudayam,
Arijit Vijey Jeyachandran, ...,
Mark S. Parcels, Arunachalam Ramaiah,
Vaithilingaraja Arumugaswami

Correspondence

arama@milwaukee.gov (A.R.),
varumugaswami@mednet.ucla.edu (V.A.)

In brief

Garcia et al. screen innate immune agonists for antiviral activity and identify that cGAS-STING cytosolic DNA-sensing pathway stimulation contributes to broader inhibition of multiple families of RNA viruses, including Zika, West Nile, Chikungunya, and SARS-CoV-2 viruses. The STING agonist cAIMP is effective in treating CHIKV-arthritis condition in a mouse model.

Highlights

- Screen identifies innate immune agonists blocking multiple families of RNA viruses
- Dectin-1 and cGAS-STING pathway agonists exhibit broader antiviral activity
- STING activator cAIMP blocks ZIKV, WNV, CHIKV, EV-D68, and SARS-CoV-2 infections
- cAIMP provides protection against CHIKV-mediated chronic arthritis in mouse model

Article

Innate immune pathway modulator screen identifies STING pathway activation as a strategy to inhibit multiple families of arbo and respiratory viruses

Gustavo Garcia, Jr.,^{1,14} Joseph Ignatius Irudayam,^{1,14} Arit Vijey Jeyachandran,¹ Swati Dubey,¹ Christina Chang,¹ Sebastian Castillo Cario,¹ Nate Price,¹ Sathya Arumugam,² Angelica L. Marquez,¹ Aayushi Shah,¹ Amir Fanaei,¹ Nikhil Chakravarty,³ Shantanu Joshi,^{4,5} Sanjeev Sinha,⁶ Samuel W. French,^{7,8} Mark S. Parcells,⁹ Arunachalam Ramaiah,^{10,11,15,*} and Vaithilingaraja Arumugaswami^{1,12,13,15,16,*}

¹Department of Molecular and Medical Pharmacology, University of California, Los Angeles, Los Angeles, CA, USA

²Department of Mathematics, Government College Daman, Daman, Dadra and Nagar Haveli and Daman and Diu 396210, India

³Department of Epidemiology, University of California, Los Angeles, Los Angeles, CA, USA

⁴Department of Neurology, University of California, Los Angeles, Los Angeles, CA, USA

⁵Department of Bioengineering, University of California, Los Angeles, Los Angeles, CA, USA

⁶All India Institute of Medical Sciences, New Delhi, India

⁷Department of Pathology and Laboratory Medicine, University of California, Los Angeles, Los Angeles, CA, USA

⁸Jonsson Comprehensive Cancer Center, University of California, Los Angeles, Los Angeles, CA 90095, USA

⁹Department of Animal and Food Sciences, Department of Biological Sciences, University of Delaware, Newark, DE 19716, USA

¹⁰Tata Institute for Genetics and Society, Center at inStem, Bangalore 560065, India

¹¹City of Milwaukee Health Department, Milwaukee, WI 53202, USA

¹²Eli and Edythe Broad Center of Regenerative Medicine and Stem Cell Research, University of California, Los Angeles, Los Angeles, CA, USA

¹³California NanoSystems Institute, University of California, Los Angeles, Los Angeles, CA, USA

¹⁴These authors contributed equally

¹⁵Senior author

¹⁶Lead contact

*Correspondence: arama@milwaukee.gov (A.R.), varumugaswami@mednet.ucla.edu (V.A.)

<https://doi.org/10.1016/j.xcrm.2023.101024>

SUMMARY

RNA viruses continue to remain a threat for potential pandemics due to their rapid evolution. Potentiating host antiviral pathways to prevent or limit viral infections is a promising strategy. Thus, by testing a library of innate immune agonists targeting pathogen recognition receptors, we observe that Toll-like receptor 3 (TLR3), stimulator of interferon genes (STING), TLR8, and Dectin-1 ligands inhibit arboviruses, Chikungunya virus (CHIKV), West Nile virus, and Zika virus to varying degrees. STING agonists (cAIMP, diABZI, and 2',3'-cGAMP) and Dectin-1 agonist scleroglucan demonstrate the most potent, broad-spectrum antiviral function. Furthermore, STING agonists inhibit severe acute respiratory syndrome coronavirus 2 (SARS-CoV-2) and enterovirus-D68 (EV-D68) infection in cardiomyocytes. Transcriptome analysis reveals that cAIMP treatment rescue cells from CHIKV-induced dysregulation of cell repair, immune, and metabolic pathways. In addition, cAIMP provides protection against CHIKV in a chronic CHIKV-arthritis mouse model. Our study describes innate immune signaling circuits crucial for RNA virus replication and identifies broad-spectrum antivirals effective against multiple families of pandemic potential RNA viruses.

INTRODUCTION

The ongoing severe acute respiratory syndrome coronavirus 2 (SARS-CoV-2) pandemic exposed the limitations and vulnerabilities of humanity from a lack of preparation to rapidly respond to a large-scale outbreak. It is difficult to accurately predict the causative agent of the next pandemic. However, based on recent epidemics over the past two decades, global climate change, the millions of individuals affected, and the continuously evolving nature of the RNA genome, arthropod-borne viruses are priority candidates. Vector-borne RNA viruses belonging to

the families Togaviridae—Chikungunya virus (CHIKV)—and Flaviviridae, such as Dengue virus (DENV), West Nile virus (WNV), and Zika virus (ZIKV), have had track records of causing epidemics.^{1–3} Daytime feeding (*Aedes aegypti* and *Aedes albopictus*) and *Culex* sp. mosquitoes are responsible for the transmission of these viral agents. The virus enters the body through a mosquito bite on the skin, inoculating the host. The virus then replicates within skin cells, specifically fibroblasts and dendritic cells (DCs). After replicating locally, CHIKV disseminates throughout the body, affecting many regions, including the lymph nodes (stromal cells, DCs, and macrophages), skeletal

muscle (satellite cells and fibroblasts),^{4,5} joints (synovial fibroblasts), brain, and liver. As a result, CHIKV infection can cause skin lesions, severe joint and muscle pain, and headaches, among other symptoms. However, due to similarities to other mosquito-borne illnesses, Chikungunya disease is often misdiagnosed as Dengue fever or Zika disease. Cardiovascular issues may also manifest from CHIKV infection, most often seen in the form of myocarditis.⁶ While symptoms can be serious, CHIKV infection is rarely lethal. ZIKV infection in women during pregnancy not only causes preterm birth and miscarriage but also causes infants to be born with microcephaly and congenital Zika syndrome.^{7,8} WNV, another member of the Flaviviridae family, is the most common arbovirus found in the United States, causing the development of serious, sometimes fatal, illnesses affecting the central nervous system, leading to encephalitis or meningitis.^{9,10}

Given their already-demonstrated epidemic potential, finding effective broad-spectrum treatments against these viruses is of the utmost importance as they become potential agents for pandemics. Mutations in the CHIKV Envelope gene (e.g., E1-A226V, E1-K211E, E2-V264A, E1-I317V),^{11,12} particularly in the Indian Ocean Lineage of the virus, have significantly increased CHIKV adaptability and infectivity. Understanding CHIKV is particularly important because it has already shown the potential to spread like wildfire in the event of even one of these mutations, particularly the E1-A226V adaptive mutation, which improved viral replication and transmission efficiency. We have seen the impact of these CHIKV mutations in epidemics and mass outbreaks in Eastern Africa,¹² South¹³ and Southeast Asia,¹⁴ and South America.¹⁵ South America, having served as a hotbed for the spread of a new variant of ZIKV in 2016,¹⁶ knows the impact that these viruses can have in terms of rapid spread and overwhelming medical infrastructure and public health efforts. ZIKV introduced the novel severe disease presentation of fetal microcephaly in infected mothers,¹⁶ the neurological consequences of which are a growing concern 7 years later as children born during that time now enter the population as schoolchildren. With the ever-present threat of climate change, the permissible habitat of mosquito vectors (*A. albopictus*, *A. aegypti*, and *Culex* sp.)¹⁷ has expanded, increasing the population that could be readily exposed to the virus.¹⁸ We have seen this in many countries, including the United States, where WNV has become endemic due to increasing winter temperatures, precipitation, and drought.¹⁸

Currently, there are no effective vaccines or therapies approved against these important pandemic potential pathogens. Thus, it is critical now more than ever to understand the host innate immune pathways and virus interactions to identify potential therapeutic targets. The mammalian innate immune pathway, more specifically the type I interferon (IFN) response, is the critical first line of defense against virus entry and replication. Pattern-recognition receptors (PRRs) recognize pathogen-associated molecular patterns (PAMPs) to induce immune responses against invading pathogens. There are four main classes of PRRs that can be split into two groups: (1) membrane-bound PRRs and (2) cytosolic PRRs. Toll-like receptors (TLRs) and C-type lectin receptors (CLRs) comprise the membrane-bound PRRs.^{19–23} TLR3, TLR7,

TLR8, and TLR9 recognize hallmark genomic components of viruses, more specifically double-stranded RNA (dsRNA), single-stranded RNA (ssRNA), and CpG DNA.^{19–21} CLRs can either stimulate the release of pro-inflammatory cytokines or inhibit TLR-mediated immune action.²² CLRs are made up of a transmembrane domain containing a carbohydrate-binding domain,¹⁹ which can recognize surface carbohydrates on viruses, bacteria, and fungi.¹⁹ Dectin-1 and Dectin-2 are common immunoreceptor tyrosine-based activation motif (ITAM)-coupled CLRs, which recognize β -glucans from fungi.²³

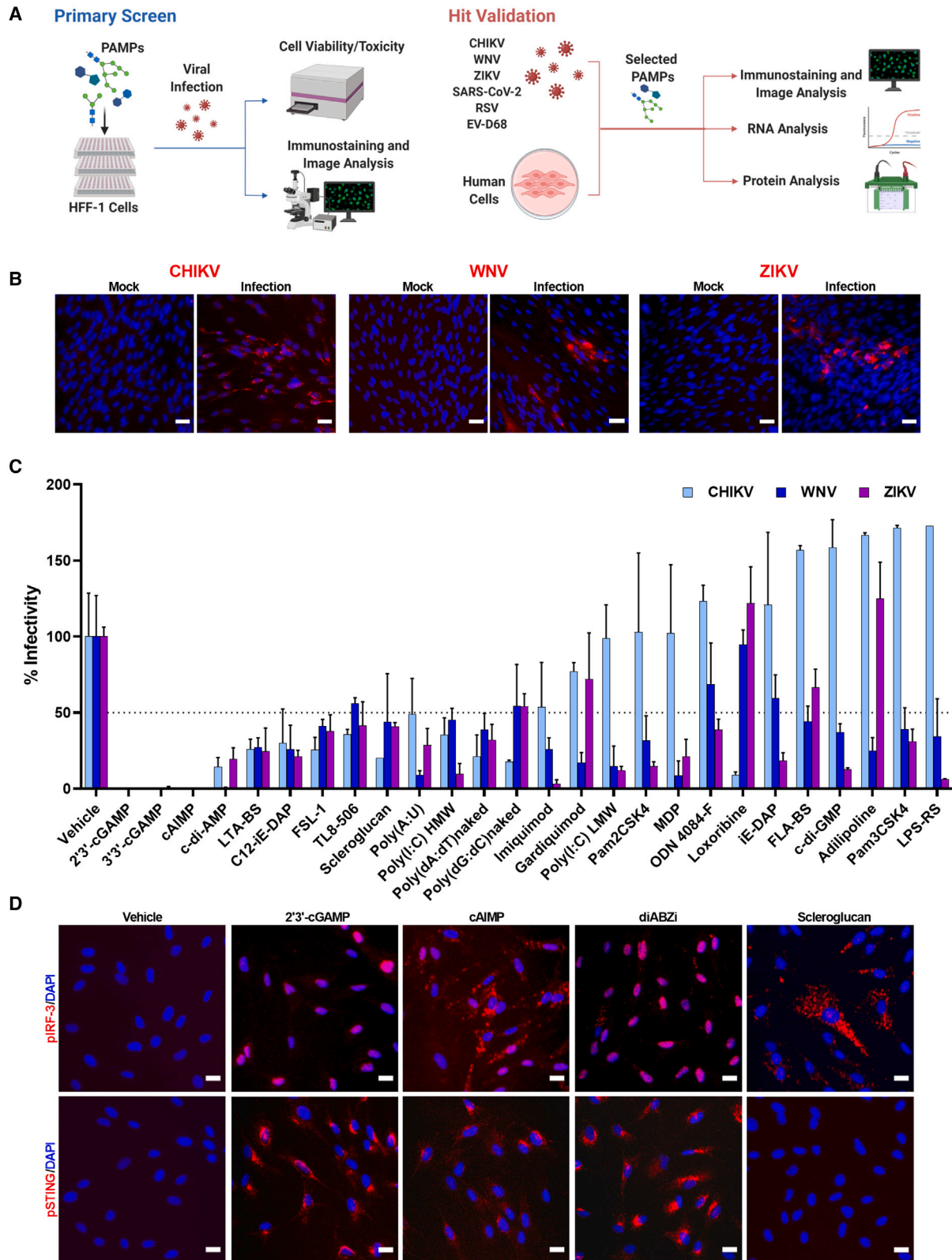
Within cells, the RIG-I-like receptor (RLR) and NOD-like receptor (NLR) families make up the cytosolic PRRs. RLRs are composed of three proteins: RIG-I, melanoma differentiation-associated gene 5 (MDA5), and DExH-Box Helicase 58 (DHX58/LGP2).^{24,25} RIG-I is an important mediator of antiviral response against CHIKV and DENV.²⁶ As opposed to TLRs, RLRs are localized in the cytoplasm. Like some TLRs, RLRs recognize dsRNA produced both as a primary genomic component of viruses and as a replication intermediate for ssRNA viruses.¹⁹ NLRs are a primary component of the inflammasome, a protein complex that activates caspase-1 and the processing of pro-inflammatory cytokines interleukin-1 β (IL-1 β) and IL-18.²⁷ NOD1 and NOD2, which have caspase activation and recruitment domain (CARD) motifs, activate nuclear factor κ B (NF- κ B) upon recognizing bacterial peptidoglycans, diaminopimelic acid, and muramyl dipeptide, respectively.^{19,28}

The cyclic GMP-AMP synthase-Stimulator of IFN genes (cGAS-STING) pathway is an essential component of the innate immune system that detects the presence of non-nucleosomal viral, bacterial, or damaged cellular cytosolic DNA. The protein cGAS is a signaling enzyme that directly binds cytosolic DNA and dimerizes upon binding to form a cGAS-DNA complex that catalyzes the synthesis of 2',3'-cGAMP from ATP and GTP.^{29,30} The STING protein dimer, a membrane receptor on the endoplasmic reticulum, binds this newly formed 2',3'-cGAMP and then recruits TANK-binding kinase 1 (TBK1), which, in turn, phosphorylates IFN regulatory factor 3 (IRF3). Several other dsDNA sensors also recognize foreign DNA (DDX41, IFI16), and this signals through interactions with cGAS to activate STING. Simultaneously, STING activation leads to IKK activation and the consequent phosphorylation and degradation of I κ B α . This results in NF- κ B1 relocating to the nucleus, along with phosphorylated (phospho)-IRF3. Subsequently, type I IFN genes and inflammatory genes are expressed, leading to antiviral and inflammatory responses. In this study, we tested the antiviral activity of various innate immune agonists that target PRRs such as TLRs, STING, NOD, Dectin, and cytosolic DNA or RNA sensors. After an initial screen in human fibroblasts cells, we validated our strongest hits that could inhibit multiple families of viruses in human cardiomyocytes and mouse models.

RESULTS

Primary screen to identify broad-spectrum antivirals

Utilizing natural and synthetic agonists targeting various PRRs, we performed a primary drug screening (Figure 1) to identify broadly acting compounds targeting members of Togaviridae (CHIKV) and Flaviviridae (ZIKV and WNV). A small library of 27



(legend on next page)

agonists was used for the primary screening. Human fibroblast cells (HFF-1) were treated with four doses of antiviral compounds in triplicate 24 h prior to infection with the above indicated viruses (Figure 1B). In parallel, drug-treated cells were subjected to viability assays to determine drug toxicity in order to select and determine non-toxic effective doses (Table S1; Figure S1). We included IFN- β as a positive control. At 48 h post-infection (hpi), infected cells were examined for viral-mediated cytopathic effect (CPE). We observed that the following 8 compounds prevented CPE: diABZI; scleroglucan; 2',3'-cGAMP; 3',3'-cGAMP; cAIMP; Poly(I:C) high molecular weight (HMW); Poly(I:C) low molecular weight (LMW); and TL8-506 (Figure S1B). At 48 hpi, infected cells were fixed and immunostained with virus-specific envelope antibodies: anti-E1 protein of CHIKV (mAb 11E7) and anti-flavivirus group E protein (monoclonal antibody [mAb] D1-4G2-4-15). Immunohistochemistry (IHC) images obtained from each well were then quantified, and the percentage of infectivity of individual compound-treated cells was obtained (Figure 1C). We found that the cells treated with the following cyclic dinucleotide (CDN) STING agonists showed below-detectable infectivity at the highest non-toxic dose (100 μ g/mL) tested against CHIKV, WNV, and ZIKV: 2',3'-cGAMP, 3',3'-cGAMP, and cAIMP (Figure 1C). Compounds such as scleroglucan (Dectin-1 agonist), c-di-AMP (bacterial CDN STING agonist), imiquimod (TLR7 agonist), and lipoteichoic acid from *Bacillus subtilis* (LTA-BS) (Gram-positive bacterial cell wall component) showed moderate antiviral activity (>50% inhibition) against all three viruses. Compounds including c-di-GMP (bacterial CDN STING agonist), MDP (NOD2 agonist), Poly(I:C) LMW, and imiquimod (TLR7 agonist) exhibited potent inhibition of WNV and ZIKV but not against CHIKV. In some instances, we observed compounds that enhanced viral replication, including Lipopolysaccharide from the photosynthetic bacterium *Rhodobacter sphaeroides* (LPS-RS), adillipoline, flagellin from *B. subtilis* (FLA-BS), and c-di-GMP (Figure 1C). Interestingly, although cells treated with the synthetic liposaccharide Pam3CSK4 were healthy across all tested concentrations, we found a dose-dependent enhancement of cell death in CHIKV-infected cells (Figures S2A and S2B).

Based on the primary screen hits, we subsequently examined the biological activities of STING agonists in activating the STING-IRF3 and STING-NF- κ B pathways, observing that STING agonists specifically induced phosphorylation of STING (Ser366) and IRF3 (Ser386) in HFF-1 cells after 2 h post-stimulation (Figure 1D), whereas scleroglucan-stimulated cells did not have detectable levels of phospho-STING. All these compounds increased NF- κ B p65 form in treated cells (Figure S1C). Taken together, we conclude that the STING agonists exhibited a broad spectrum of antiviral activity against RNA viruses by stimulating innate immune pathway.

Validation of antiviral hits from the primary screen

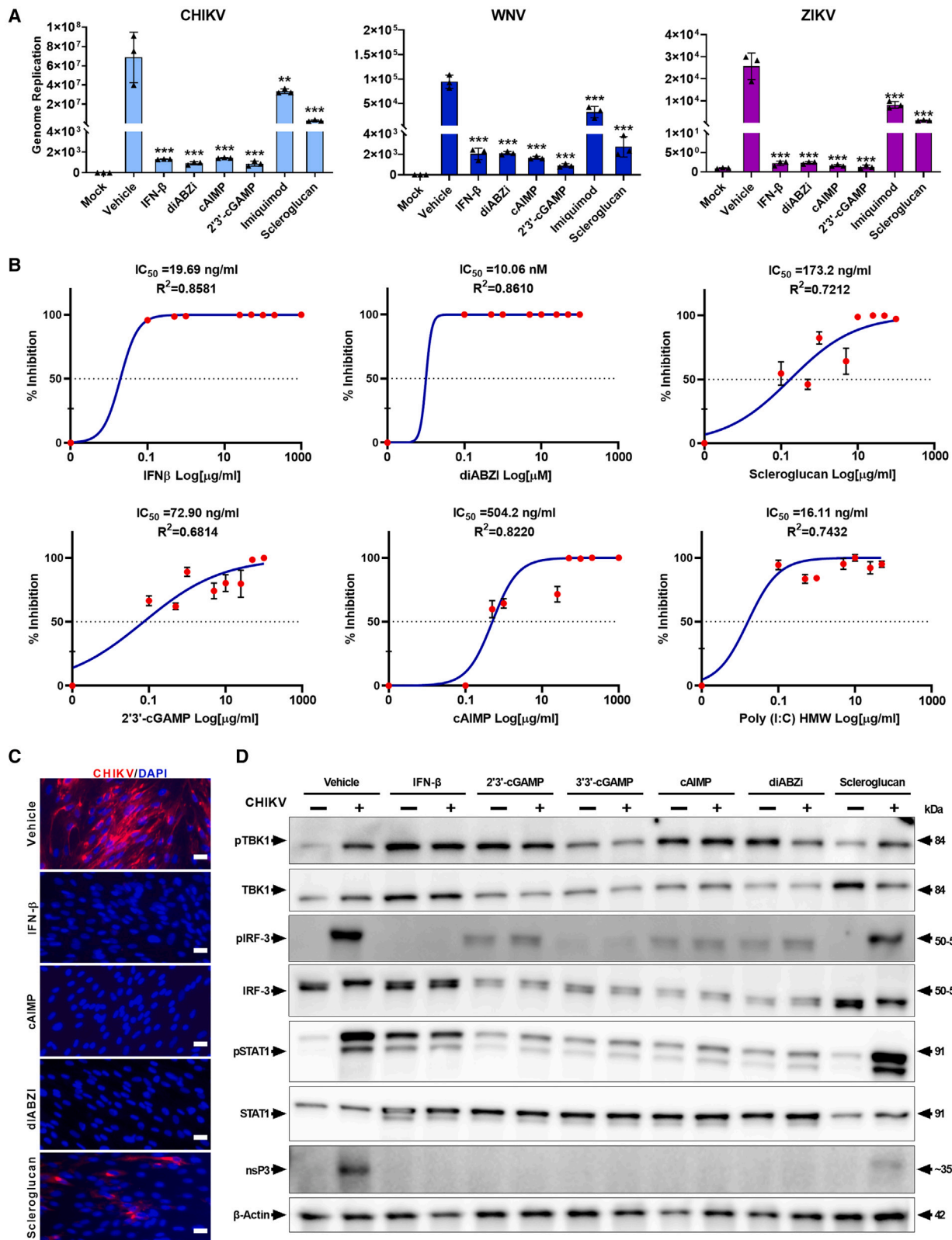
Subsequently, we carried out a secondary confirmation using a sensitive qRT-PCR assay to evaluate genome replication of these arboviruses in drug-treated cells (Figure 2A). Our data demonstrated that the selected STING agonists (diABZI, cAIMP, and 2',3'-cGAMP), the TLR7 agonist (imiquimod), and scleroglucan significantly reduced viral genome replication, which was also confirmed by quantifying the viral titer (Figure S2). Thereafter, a dose-response study was used to determine the half-maximal inhibitory concentration (IC₅₀) of antiviral compounds in human fibroblasts (Figure 2B). We focused on CHIKV, a less well-characterized RNA virus, for subsequent validation of PRR agonists, particularly ligands for STING, TLR3, and Dectin-1. STING is the downstream signaling activator of cGAS-mediated cytosolic DNA-sensing pathway, and TLR3 (dsRNA) is an endosomal RNA sensor.³¹ Compounds 2',3'-cGAMP, Poly(I:C) HMW, scleroglucan, and cAIMP demonstrated antiviral activity at an IC₅₀ <500 ng/mL (Figure 2B). Positive control IFN- β and drug-like non-CDN STING agonist diABZI showed IC₅₀ values of 19.69 ng/mL and 10.06 nM, respectively. We also observed that post-treatment of CHIKV-infected cells (2 hpi) with cAIMP and diABZI demonstrated potent antiviral activity (Figure S2). Consistent with virulent CHIKV results, a CHIKV vaccine strain (181/25) was also inhibited by STING agonists in the HFF-1 cells (Figure S2). Representative IHC images of drug-treated and CHIKV-infected fibroblasts at an effective antiviral dose are shown in Figure 2C. To understand the mode of action of these antiviral compounds, we performed a comprehensive analysis of the innate immune signaling pathway using western blots of HFF-1 cells stimulated by selected STING agonists either with or without CHIKV infection (MOI: 0.1) at 24 hpi (Figure 2D). In the uninfected cells, we found that pretreatment with the STING agonists cAIMP, diABZI, 2',3'-cGAMP, and 3',3'-cGAMP induced phosphorylation of IRF3. Notably, the cells pretreated with STING agonists had a reduction in total IRF3 levels at 24 hpi. IFN- β strongly induced phospho-TBK1 (Ser172) and phospho-STAT1 (Tyr701). Compared with the STING agonists, scleroglucan-treated cells had only the basal level of phospho-IRF3, indicating specificity and differential mode of actions between agonists and their associated PRRs. CHIKV nsP3 protein level was consistent with antiviral activity of the tested compounds. Taken together, we conclude that STING-mediated activation of the TBK-IRF3 signaling cascade exerts potent antiviral activity against CHIKV.

Comparative transcriptomics study on arboviruses treated with STING agonist

Based on our validation data, we selected the synthetic CDN cAIMP for further mode-of-action studies in the context of arboviral infections using a systems-level transcriptomics approach.

Figure 1. Broad-spectrum antiviral screen

(A) Schematic of antiviral screen performed using molecules modulating PAMPs.
(B) Immunofluorescence images of human fibroblasts (HFF-1) infected with indicated viruses are shown. CHIKV (MOI: 0.1) and ZIKV (MOI: 0.1) or WNV (MOI: 1) were detected by anti-E1 protein and anti-flavivirus E protein antibodies, respectively. Scale bar: 25 μ m.
(C) Graph shows the percentage of infectivity of various compounds targeting CHIKV and flaviviruses. Horizontal dotted line indicates 50% infectivity.
(D) Immunofluorescence images show phospho-IRF3 (S386) and phospho-STING (S366) in fibroblast after 2-h post-stimulation with indicated compounds. Note: scleroglucan-stimulated cells do not have detectable level of phospho-STING, and only a few cells have a cytoplasmic form of phospho-IRF3. Scale bar: 10 μ m. See also Figures S1 and S2 and Table S1.



(legend on next page)

To uncover the dysregulated pathways in HFF-1 cells infected with these pandemic potential RNA viruses—CHIKV, WNV, and ZIKV (MOI: 0.1)—we performed total RNA sequencing analysis of vehicle- or cAIMP-treated virus-infected HFF-1 cells. The cells were pretreated with the vehicle (saline), cAIMP (100 $\mu\text{g}/\text{mL}$), or scleroglucan (50 $\mu\text{g}/\text{mL}$), and 24 h later, viral infection was carried out. Subsequently, at 24 hpi, the cells were harvested for RNA sequencing analysis (Illumina NGS), revealing that the transcriptional responses in CHIKV-infected cells were significantly different from the host response in WNV- and ZIKV-infected cells (Figures 3A and 3B). The expressions of host genes in CHIKV-infected cells were increased about 96- and 33-fold compared with WNV- and ZIKV-infected cells, respectively, reflecting the differential nature of the pathogenesis mechanism of these viruses and the associated host responses. Because scleroglucan-treated/viral-infected cells had only a few differentially regulated genes, we mainly focused on cAIMP-treated samples for further analysis. While similar numbers of host genes were expressed in either vehicle- or cAIMP-treated CHIKV-infected cells, distinctive patterns of transcription was observed (Figure 3A). However, host gene expressions were increased 32- and 6-folds in WNV- and ZIKV-infected cells treated with cAIMP compared with the vehicle-treated infected cells, respectively. This demonstrates a uniform antiviral response of cAIMP in host response to different viral infections. Considering the different levels of host transcriptional response to these vehicle- and cAIMP-treated viral infections, only 3 (*OAS2*, *IFI44L*, and *HELZ2*) and 74 genes, respectively, were commonly upregulated (Figure 3B). These 74 common genes could potentially be drug-specific elements contributing to the broad-spectrum antiviral process (Table S3). Among cAIMP-treated/virus-infected cells, the majority (88%) of the upregulated genes in ZIKV-infected cells were also upregulated in WNV-infected cells, suggesting that several molecular functions are commonly pursued by these two flaviviruses compared with the alphavirus CHIKV.

We performed a sensitive qRT-PCR analysis to quantitatively assess the levels of each target gene in the STING signaling pathway following infection and treatment with drug compounds (Figures 3C and S3A). These data revealed that CHIKV and WNV activated STING pathway genes, including *cGAS*, *IFI16*, and *TRIM21*, at 48 hpi. Moreover, all three arboviruses upregulated type I IFN-stimulated genes *OAS2* and *IFI44L*. Both these STING and type 1-IFN pathway genes were transcriptionally induced in cAIMP-treated/viral-infected cells. In general, many of these innate immune pathway gene expressions were reduced by treatments with either cAIMP or scleroglucan, which could possibly be due to inhibition of virus replication in treated cells (Figures 3C and S3A). Furthermore, we have provided the results of the expression patterns of STING pathway genes

from the comparative transcriptome dataset for these arboviruses at an early time point of 24 hpi (Figure S3B). Many STING pathway genes were differentially regulated in CHIKV-infected cells compared with ZIKV- or WNV-infected cells. Furthermore, in response to these virus infections, the host cells upregulated various pathways, including IFN signaling pathways and NF- κ B and immune cytokine signaling pathways, as well as virus-specific pathways, such as DNA damage/telomere stress-induced senescence (CHIKV), zinc influx into cells by the SLC39 gene family (WNV), and UNC93B1-deficiency herpes simplex virus type 1 encephalitis (HSE) (ZIKV) (Figure 3D; Table S2). While cAIMP-treated/virus-infected cells primarily triggered many antiviral immune responses, we observed distinct upregulation of genes in the cell cycle and transcription pathways in cAIMP-treated/CHIKV-infected cells (Figure 3E; Table S2). A complete list of pathways enriched during virus infections in the context of drug treatment is provided in the Table S2. These results indicate that CHIKV contributes to robust transcriptional dysregulation in fibroblasts compared with WNV and ZIKV, reflecting a possible difference in the disease pathogenesis mechanisms by alphaviruses and flaviviruses despite all being mosquito-borne viruses. Irrespective of the observed differences in molecular signatures, the STING agonist demonstrated a broader inhibition against these arboviruses.

Pharmacogenomics study on STING and Dectin-1 agonists against CHIKV

We further performed an in-depth transcriptomics study to compare the antiviral efficacy of synthetic CDN cAIMP and scleroglucan in CHIKV-infected HFF-1 cells. To uncover the dysregulated pathways in CHIKV-infected (vehicle-treated) as well as drug-treated infected cells, we performed total RNA sequencing analysis at 24 hpi. The transcriptome data reveal that viral genome reads comprised 83% of the total reads for vehicle-treated cells, 63% for scleroglucan-treated cells, and 0.1% for cAIMP-treated cells, concurrent with the observed antiviral phenotype (Figure 4A). Viral count analysis showed uniform increases in expression of all viral genes (structural and non-structural) in CHIKV-infected cells. However, viral gene expression was reduced about 880-fold in cAIMP-treated infected cells compared with untreated infected cells (Figure 4B). RNA sequencing analyses indicated that the transcriptional response in CHIKV-infected cells is significantly different from the host response to the agonists, especially for cAIMP, which further explains their extreme coordinates on the principal-component analysis (PCA) plot (Figure 4C). Moreover, treatments with cAIMP in uninfected and infected cells show very similar transcriptional responses, though they are different from scleroglucan-treated cells (Figures 4A–4E). In vehicle-treated cells, viral RNA approached 83% of total RNA reads at 24 hpi, which

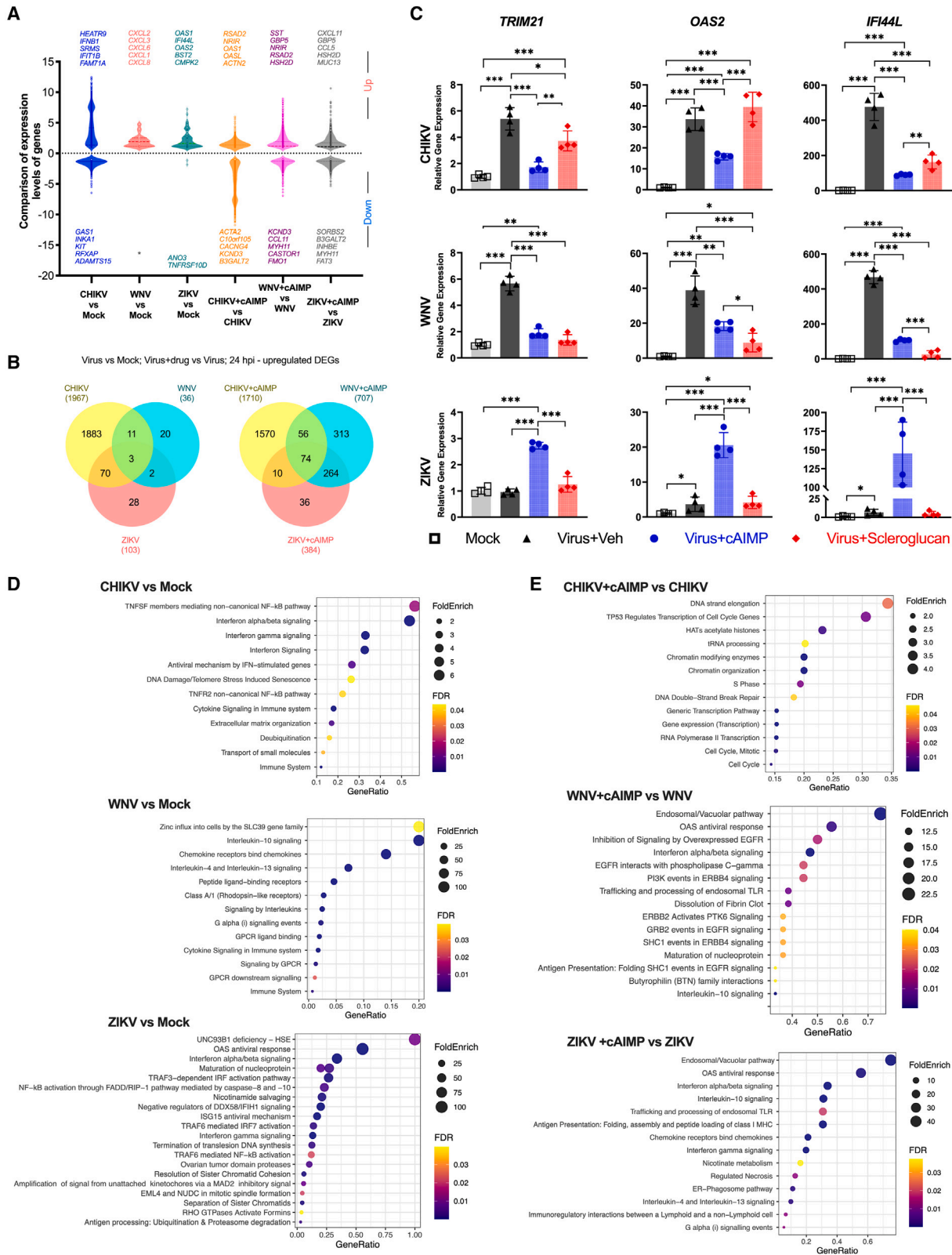
Figure 2. Hit validation and mode-of-action studies

(A) qRT-PCR analysis of viral genome replication in drug treated fibroblasts at 48 hpi with indicated arboviruses. Student's t test. * $p > 0.01$, ** $p > 0.001$, *** $p > 0.0001$.

(B) Dose-response curve of compounds showing antiviral activity against CHIKV. IC_{50} and R^2 values are included for each compound.

(C) Representative immunofluorescence images of indicated drug-treated and CHIKV-infected human fibroblasts at 48 hpi are shown. Scale bar: 25 μm .

(D) Western blot analysis of innate immune pathway of cells stimulated with various STING agonists, with or without CHIKV infection, at 24 hpi. The Dectin-1 agonist scleroglucan is included as an additional control.



(legend on next page)

clusters apart from drug-treated RNA samples, reflecting an overall difference in host response (Figures 4C–4E). With regard to different levels of CHIKV gene expression in treated infected cells (Figure 4B), the host transcriptional response to CHIKV infection and cAIMP-treatment CHIKV infection are differential in nature (Figure 4E), with only 39 and 230 shared down- and up-regulated genes, respectively (Figure 4G), suggesting that genes involved in only certain molecular functions are commonly shared by two conditions. However, cAIMP-treated CHIKV-infected cells had 284 distinctive differentially expressed genes that could potentially be drug-specific elements contributing to the antiviral process. Pathway and Gene Ontology enrichment analyses of virus-infected cells treated with cAIMP showed upregulation of many cell repair mechanisms, including histone acetyltransferase (HAT) activity, DNA double-strand break repair, and metabolic pathways of amino acids and their derivatives (Figure S4). Additionally, cAIMP-treated (uninfected cells) exhibited upregulation of multiple antiviral and metabolic pathways, including negative regulation of DDX58/IFIH1 signaling and nicotinate metabolism, which are downregulated in CHIKV-infected cells (Figures 4H and S4). Analysis of differentially regulated genes in various experimental conditions showed that HEAT Repeat Containing 9 (*HEATR9*) is highly upregulated in CHIKV-infected cells (Figure 4F), and cAIMP treatment reversed the induction of this gene. The *HEATR9* gene has been shown to regulate cytokine production³² with mutations reported in patients with POEMS (polyneuropathy, organomegaly, endocrinopathy, monoclonal gammopathy, skin changes) syndrome, a plasma cell dyscrasia.

In response to CHIKV infection and cell injury, the infected cells upregulated various pathways including the tumor necrosis factor (TNF) receptor superfamily-mediated NF- κ B, DNA-damage/telomere stress-induced senescence, and immune cytokine and type I IFN signaling pathways (Figures 3D and 4H; Table S2). However, cAIMP treatment primarily activated antiviral innate immune responses (Figure S4). Interestingly, cAIMP treatment resulted in the upregulation of nicotinate metabolic pathway (Figure 4I). Functional validation by intracellular metabolite analysis confirmed that cAIMP treatment increased nicotinamide adenine dinucleotide (NADH) levels (Figure 4J). NADH can help provide energy to execute the antiviral responses. Similarly, cAIMP treatment prevented ATP depletion, likely by inhibiting virus replication. We have observed phosphorylation of STING during CHIKV infection, suggesting activation of the STING pathway as well as the downstream IRF3-IFN-STAT1 pathway in human (rhabdomyosarcoma [RD]) muscle cells (Figure 4K). Taken together, our

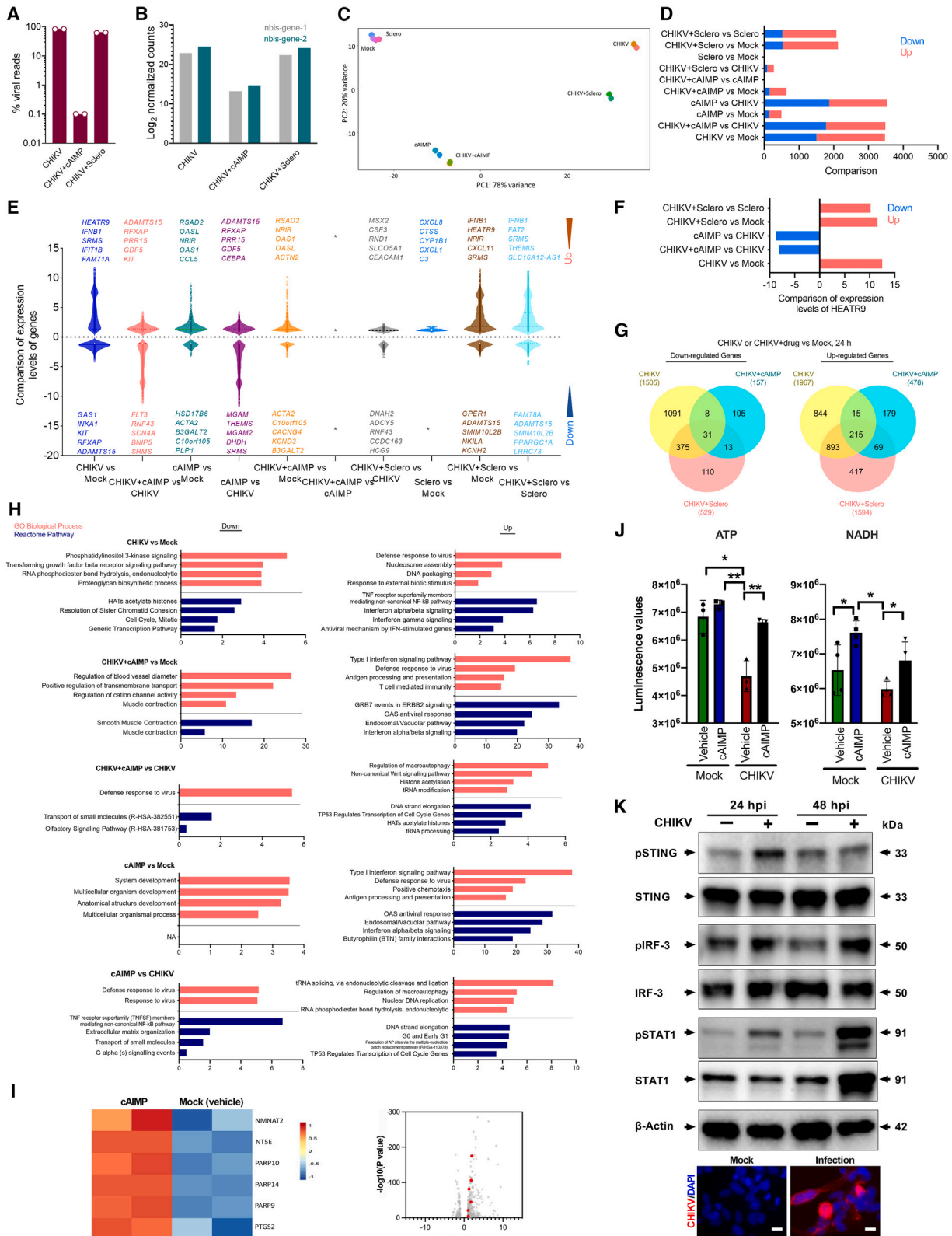
comprehensive transcription analysis and validation revealed specific mode of action for cAIMP treatment and pathophysiological molecular changes during CHIKV infection.

Antiviral compounds prevent viral infection of cardiomyocytes

Cardiovascular involvement has been shown to be a common manifestation of CHIKV infection.⁶ In addition, other viral-mediated cardiovascular diseases among RNA viral infections have been reported. Human patients have been shown to develop myocarditis and pericarditis after subsequent WNV and enterovirus-D68 (EV-D68) infections.^{33,34} Recently, it has been shown that SARS-CoV-2 is responsible for multiple cardiovascular (CV) manifestations^{35–37} and can infect human cardiomyocytes.^{38,39} Therefore, assessing a broad spectrum of antivirals in a relevant cardiomyocyte system can help determine the effectiveness of these compounds. We first evaluated the susceptibility of cardiomyocytes to viral infections using a human pluripotent stem cell-derived cardiomyocyte (PSC-CM) system (Figure 5A). We have previously shown that SARS-CoV-2 can establish active infection in PSC-CMs.^{38,40} We observed that CHIKV established productive infection in PSC-CMs, which was inhibited by scleroglucan treatment (Figure S5A). For detailed study, we also included additional respiratory pathogens, namely respiratory syncytial virus (RSV) and EV-D68. The PSC-CMs were infected with various viruses. At 48 hpi, the cells were fixed with 4% paraformaldehyde and immunostained with antibodies targeting each virus-specific antigen (key resources table). Immunohistochemistry (IHC) analysis indicated that the CMs are highly susceptible to CHIKV, WNV, and EV-D68 infections but not RSV (Figure 5A). Using this platform, we subsequently tested STING agonists cAIMP and diABZI, as well as IFN- β and remdesivir, against these arbo- and respiratory viruses (Figure 5B). The STING agonists demonstrated potent antiviral activity across all tested RNA viruses in the biologically relevant human PSC-CMs. These agonists induced phosphorylation of STING in PSC-CMs, indicating the activation of a STING-mediated antiviral signaling cascade (Figure S5A). Interestingly, the STING agonists were not effective against RSV in human A549 lung epithelial cells. However, IFN- β , remdesivir, and 6-azauridine demonstrated efficient inhibition of RSV infections (Figures 5C and S5C). Remdesivir, a well-known RNA-dependent RNA polymerase inhibitor approved for SARS-CoV-2 treatment, had no effective antiviral activity against CHIKV or WNV. Taken together, the STING agonists exhibited broad-spectrum antiviral activity against both arbo- and respiratory viruses in cell culture models.

Figure 3. Comparative transcriptome analysis of drug-treated and arbovirus-infected human fibroblasts

(A) Violin plot shows comparative analysis of differentially expressed genes of vehicle- or cAIMP-treated virus-infected HFF-1 cells at 24 hpi. (B) Venn diagrams display the number of common and distinctive genes upregulated in virus-infected cells (left) as well as in cAIMP-treated virus-infected cells (right) at 24 hpi (false discovery rate [FDR] < 0.01 and log₂ fold change [log₂FC] > 1). (C) Graphs show qRT-PCR analysis of innate immune STING pathway genes in arbovirus-infected fibroblasts at 48 hpi with or without drug treatments of infected cells. Student's t test. *p > 0.01, **p > 0.001, ***p > 0.0001. (D and E) Dot plot analysis of overrepresented pathways in viral-infected (D) and cAIMP-treated virus-infected cells (E). The size of the dot represents the fold enrichment (FoldEnrich), while its color represents the FDR (p adjusted) value for each enriched Reactome pathway. The x axis represents the percentage of upregulated genes in the selected pathway that is presented in the y axis. See also Figure S3 and Tables S2 and S3.



(legend on next page)

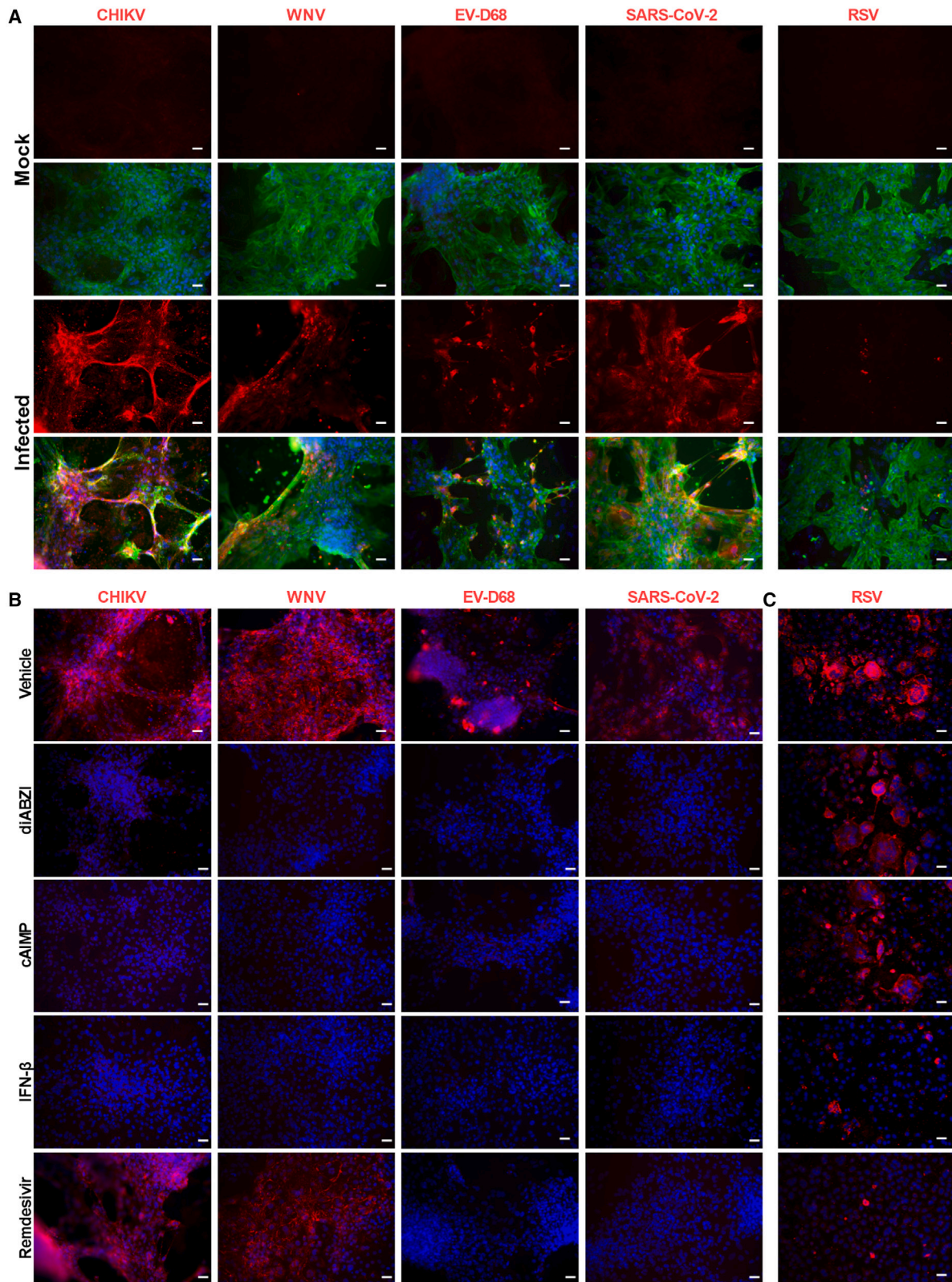
cAIMP provides therapeutic benefit in treating CHIKV arthritis in mouse model

Next, we evaluated the antiviral effect of cAIMP, a synthetic CDN, in a preclinical mouse model of CHIKV.^{41,42} This potent antiviral compound cAIMP, an analog of natural 3'3'-cGAMP, is derived with adenine and inosine nucleosides. The schematic of both prophylactic and therapeutic animal study designs is provided in Figure 6A. For prophylactic study, the mice (14 months old, C57BL/6J) were systemically pretreated with a single dose of cAIMP (10 mg/kg) by intraperitoneal injection at day -1. The control group received a saline injection as a placebo treatment. 24 h later, a group of cAIMP- or saline-administered animals (n = 5) were sacrificed, and the left footpad tissues were harvested for gene expression analysis. The cAIMP-treated animals had significant activation of the STING pathway and the antiviral genes *Trim21* and *Oas1* (Figure 6B). In parallel at 24 h post-treatment (hpi), additional groups of mice were inoculated with CHIKV (strain 181/25) in the left rear footpad by subcutaneous injection. The animals were observed for the next 7 days for body weight changes and clinical signs of footpad swelling (Figures 6C and S6A). CHIKV infection did not have a deleterious effect on overall animal health, as the infected animals maintained body weight throughout the study. We observed that a single dose of prophylactic cAIMP treatment significantly prevented CHIKV-mediated footpad swelling, whereas the thickness of the viral-inoculated left-rear footpad was increased in the saline-treated animals (Figure 6C). During the acute phase of infection on day 3, mice were sacrificed, and the viral titer in the inoculated left-rear footpad was measured by qRT-PCR (Figure 6C). We have observed that the cAIMP pretreatment resulted in 2 log reduction in viral genome replication. Transcriptomics analysis of left-rear footpad at 7 days post-infection (dpi) revealed that transcriptional differences in untreated (648 differentially expressed genes [DEGs]) and cAIMP-treated (1,183 DEGs) CHIKV-infected animals (Figures 6D and S6D)—a similar pattern as was observed in our analysis of human HFF-1 cells. The mouse transcriptional responses were increased almost 2-fold

in cAIMP-treated CHIKV-infected animals compared with the saline-treated CHIKV-infected animal. This indicates a robust antiviral host response induced by cAIMP in CHIKV-infected footpad. Transcriptome analysis also revealed that CHIKV infection activated several biological pathways involved in IFN- γ signaling, antimicrobial proteins, and platelet adhesion. Compared with the saline-treated/CHIKV-infected mice group, cAIMP-treated mice showed upregulation of myogenesis and metabolic pathways involved in keratan sulfate, chondroitin sulfate, and angiotensin conversion; meanwhile, downregulation of NLRP3 inflammasome, pyroptosis, and various IL signaling pathways was observed (Figure 6D; Table S2). Histopathological analysis revealed that the saline group had heavy infiltration of inflammatory cells in the footpad muscle, skin, and joint tissues, resulting in myocytis, dermatitis, and arthritis at 7 dpi (Figure 6E). The synovial cavity of the affected joint had fibrinous exudate. In addition, the synovial membrane lining the joint synovial cavity was heavily infiltrated with mononuclear inflammatory cells (Figures 6E and S6B). Furthermore, IHC analysis revealed that the saline-treated/CHIKV-infected left footpad had heavy infiltration of mononuclear cells including macrophages, CD4⁺ helper T cells, and CD8⁺ cytotoxic T cells. The observed pathological changes and left-rear footpad swelling were prevented upon cAIMP administration. These gross and histopathological results were supported by significant downregulation of the expression of inflammatory genes *Ccl2*, *Il-6*, and *Il-10* in the left footpad of the cAIMP-pretreated group at 7 dpi (Figure S6C). The contralateral right-rear footpad volumes were not changed relative to the inoculated left-rear footpad, suggesting that the infection is predominantly localized (Figure S6E). In a chronic long-term follow-up study up to 2 months post-infection using 14-month-old animals, cAIMP pretreatment had significantly reduced the volume of footpad swelling as well as virus replication (Figure S6F). This long-term study showed that CHIKV can establish a chronic persistent infection in the older mice. These observations indicate that STING pathway induction exerts a strong antiviral response *in vivo*.

Figure 4. Transcriptome analysis of control and drug-treated/CHIKV-infected human fibroblasts

- (A) Bar graph shows proportion of total reads comprising CHIKV transcripts in indicated treatments. The proportion of virus-aligned reads over total reads is shown for each sample. Error bars represent average (\pm SD) from two biological replicates.
- (B) Normalized read counts (\log_2) of CHIKV RNA products, showing transcriptional enrichment of viral genes in CHIKV-infected cells when compared with uninfected cells. The infected cells treated with cAIMP drug showed much less viral enrichment.
- (C) Principal-component analysis for the global transcriptional response to CHIKV infection and drug cAIMP or scleroglucan treatment.
- (D) Identification of the number of down- and upregulated genes in different samples.
- (E) Comparison of expression levels of differentially expressed genes in different samples. A greater number of genes were upregulated in CHIKV-infected cells, while a greater number of genes were downregulated in cAIMP-treated/CHIKV-infected cells.
- (F) Comparison of expression levels of HEATR9 in different samples.
- (G) Venn diagram displays the number of common and distinctive genes down- and upregulated in various conditions. CHIKV-infected cells had greater numbers of down- and upregulated genes. The CHIKV-infected cells treated with cAIMP had the least number of genes down- and upregulated.
- (H) *In silico* functional annotation of differentially expressed gene sets in different samples performed using PANTHER, and the four most overrepresented GO Biological Process (orange) and Reactome pathway (blue) terms are shown.
- (I) Heatmap and volcano plot (red; FDR < 0.01 and \log_2 FC > 1) of upregulated genes in nicotinate metabolic pathway in cAIMP-treated cells. Heatmap illustrates Z scores as expression levels of these 6 differentially expressed genes (DEGs). Red color represents genes upregulated in cAIMP-treated alone cells compared with control cells.
- (J) Graphs show intracellular ATP and NADH metabolites of uninfected and CHIKV-infected cells, with or without cAIMP treatment at 48 hpi. Student's t test. *p > 0.01, **p > 0.001. n = 2 independent experiments.
- (K) Western blot analysis of STING-IRF3 innate immune pathway activation in CHIKV-infected human RD muscle cell line. Immunofluorescence images show CHIKV infection in fibroblasts at 48 hpi. Scale bar: 10 μ m.
- See also Figure S4.



(legend on next page)

Subsequently, we evaluated the efficacy of cAIMP in a therapeutic capacity. The mice were infected with CHIKV in the left-ear footpad and treated with a single dose of cAIMP (10 mg/kg) either at 6 or 12 hpi via systemic intraperitoneal route (Figure 6F). The animals were observed up to 21 dpi for clinical signs of footpad swelling and body weight change. Similar to the prophylactic countermeasure, we noticed that the cAIMP treatment has protected the animals from significant footpad swelling by reducing viral replication (Figure 6F), inflammatory gene expression, and inflammatory cellular infiltration (Figure S7). Taken together, the STING agonist cAIMP has demonstrated potent prophylactic and therapeutic efficacy against CHIKV arthritis.

DISCUSSION

The objective of this study was to identify broadly acting antivirals against pandemic potential arthropod-borne viruses. Importantly, we observed that agonists of the cGAS-STING cytosolic DNA-sensing pathway exhibited potent antiviral activity against members of multiple sense strand RNA viral families. STING is a core component of the cytosolic DNA-sensing pathway. However, the mechanism of STING pathway-mediated antiviral response against RNA viruses is not clear. STING can be involved in sensing RNA viruses through cross-talk with the RNA-sensing RIG-I-MAVS pathway and mitochondria DNA leakage in infected cells.^{43–49} In *Drosophila melanogaster*, cGAS-like receptors have been described for sensing RNA sequences and activating the STING pathway.⁵⁰ There may have been cGAS-like receptors in mammalian cells that can recognize viral RNA. Deficiency of cGAS and STING in the embryonic fibroblasts of golden ticket mice (I199N missense mutation in *Sting* resulting in lack of IFN- β production following STING agonist stimulation) saw significantly exacerbated infection by CHIKV, suggesting that the cGAS-STING pathway may play a role in the attenuation of chikungunya disease. This finding supports previous work demonstrating its role in the restriction of alphavirus replication.^{51–54} The CHIKV nsP1 protein, a non-structural protein of CHIKV that anchors to cell membranes, has also been found to interact directly with STING. This interaction elucidates an important immune evasion role of nsP1 in disrupting STING dimerization and resultant dampening of STING-mediated immune response to CHIKV infection.^{51,55–57} The CHIKV capsid protein was found to induce autophagy-dependent degradation of cGAS, leading to downregulation of IFN- β transcription.⁵⁸ Moreover, a previous study has shown that Sindbis virus nsP4 is degraded by the proteasome.⁵⁹ In this context, observed interactions between CHIKV nsP4 and cGAS⁵¹ may lead to partial cGAS degradation via the proteasome. However,

there is no direct evidence to support this. Beyond demonstrating the immune-dampening potential of CHIKV, this observation reveals a direct evolutionary mechanism within the RNA virus that targets the cGAS-STING pathway, thus emphasizing the need to better understand the role of cGAS-STING in the modulation of CHIKV-induced arthritis and myositis. We have observed that stimulation of this pathway with both natural and synthetic STING-activating compounds overcomes CHIKV-mediated immune evasive mechanisms. Moreover, STING agonists have been shown to exert antiviral activity against SARS-CoV-2.⁶⁰ There is a possible explanation for STING agonists having a stronger RNA antiviral effect due to the evolving nature of these viruses to evade the RNA-sensing RIG-I-MDA5-mediated IFN activation pathway. This evolutionary imbalance can be potentially exploited by stimulating the cGAS-STING DNA-sensing pathway as an effective antiviral strategy. In addition, evidence suggests that STING-activating compounds can be useful in mediating a robust immune response as adjuvants in vaccines against viral infections (HIV, influenza, and coronaviruses) and can be used as initiators of anticancer immunostimulatory effects.^{61,62} This avenue for constructing effective vaccines is possible due to stimulation of the cGAS-STING pathway and activation thereafter of IRF3, NF- κ B, type I IFNs, and other pro-inflammatory cytokines that help modulate antigen presentation and immune responses.^{61,63–66}

In comparing the genome replication and transcriptome of CHIKV with other viruses, we observed a higher number of gene dysregulations and a higher viral load. This finding suggests that CHIKV displays faster replication kinetics in our *in vitro* models than WNV or ZIKV. Even in cases of coinfection with other viruses, such as DENV and ZIKV, CHIKV replication has been found either to not be affected⁶⁷ or to result in decreased replication⁶⁸ of the coinfecting virus. Our finding has been substantiated in other studies,^{67,69,70} suggesting a ready path to widespread infection and greater pandemic potential for CHIKV.

Interestingly, we observed that the Dectin-1 ligand scleroglucan exhibited antiviral activity by preventing infection of arboviruses in fibroblasts, as well as moderately reducing CHIKV replication in PSC-CMs. The mode of action of this activity is independent of the STING-IRF3-STAT1 type I IFN pathway. Transcriptomics analysis confirmed that scleroglucan can only stimulate the inflammatory pathway. Compared with the STING agonist, cAIMP activated the type I IFN signaling pathway and defense response against the virus. Additionally, gene knockdown experiments can provide valuable insight into the key genes involved in antiviral response triggered by these compounds against the tested RNA viruses. We have noticed that the compound Pam3CSK4, a synthetic triacylated lipopeptide⁵⁷ ligand of TLR2/TLR1, had a

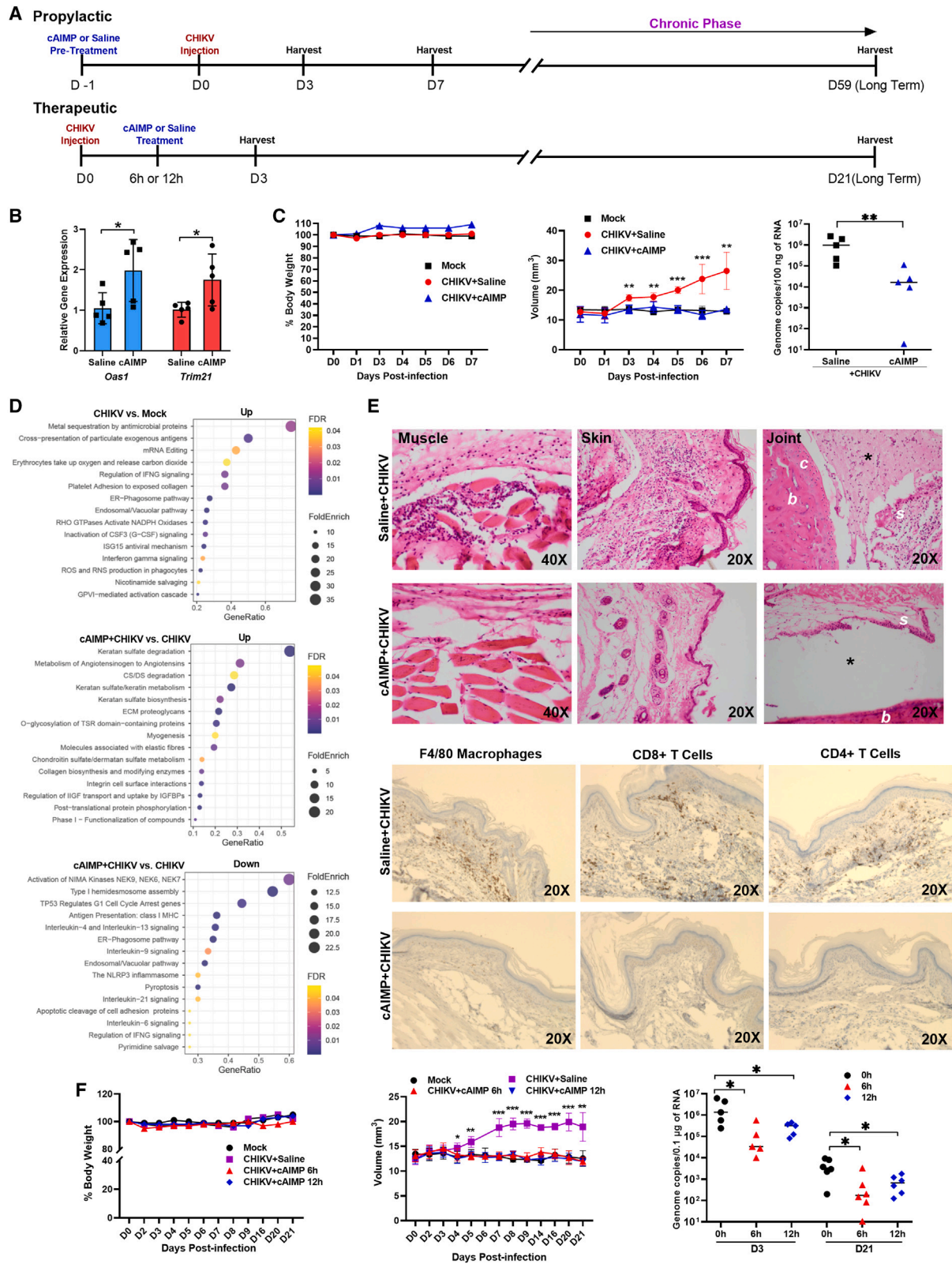
Figure 5. Evaluating the susceptibility of PSC-CMs to different families of RNA viruses and testing broad-spectrum antiviral therapeutic efficacy

(A) IHC images depict infected PSC-CMs with indicated RNA viruses, EV-D68 (anti-VP1 protein), SARS-CoV-2 (antispikes protein), and RSV strain A2001/3–12 (antifusion protein), and cardiac-troponin I (green). Scale bar: 25 μ m. Note: RSV is not efficient in infecting cardiomyocytes.

(B) IHC images present antiviral activity of tested compounds. STING agonists and IFN- β have potent antiviral activity across all tested RNA viruses. Remdesivir is not active against CHIKV and WNV. Scale bar: 25 μ m

(C) Immunofluorescent images present RSV-infected AF49 lung epithelial cells at 48 hpi. Note: IFN- β and remdesivir demonstrated efficient inhibition of RSV infection. Scale bar: 25 μ m. Representative data from n = 2 independent experiments are provided.

See also Figure S5.



(legend on next page)

dose-dependent enhancement of cell death in CHIKV-infected cells, although the compound alone has no toxicity. This observation indicates that, in this cell type, CHIKV infection can be aggravated in the presence of bacterial cell wall components. Thus, it is possible that comorbidities, particularly those attributed to bacterial infections, can stimulate a signaling cross-talk that might trigger apoptosis and/or cell injury.

Moreover, we have provided evidence that CHIKV, WNV, and EV-D68 pathogens can directly infect human heart cells. This reveals an important discovery of a biologically relevant platform to understand the pathogenic mechanism of CV complications caused by these viruses and to evaluate additional antiviral agents. The tested negative-strand RNA virus RSV has not shown tropism for CMs and was not inhibited by STING agonists in transformed lung cells. Despite RSV having some association with sinoatrial blocks and transient rhythm alterations,⁷¹ there was no direct infection of PSC-CMs. Thus, it is possible that the CV effect could be a direct outcome of RSV pulmonary infection. Additional studies are required to delineate these heart tropisms and STING pathway interactions with RSV. Moreover, given our observation that while many RNA viruses were inhibited by STING agonists, the negative-sense RNA virus RSV resisted this inhibition. This observation of differential sensitivity sets the stage for future mechanistic studies to better define viral-specific factors that may be involved in host immune evasion through antagonizing STING pathway activation. Viral variants evading antiviral responses mounted by STING agonists can be a concern. These specific drug-resistant variants can be identified and characterized by performing serial viral passage experiments in the presence of STING agonists.

In this study, we have utilized a chronic arthritis mouse model. The compounds can be further evaluated in CHIKV mouse models of different ages, genetic backgrounds, and organ-specific interventions. For acute lethal studies, neonatal and immunocompromised mice models can be utilized.^{72–74} We verified a single-dose regimen for *in vivo* efficacy against CHIKV in a prophylactic and therapeutic setting. Further studies are required to evaluate a multiple-dose regiment of the STING agonists and additional compounds across multiple RNA viruses in animal models to optimize treatment conditions. The drug formulations can be developed for oral,

inhalational, and topical modes of treatment. We have demonstrated in a CHIKV *in vivo* model that there is long-term viral persistence for months. Therefore, further studies are required to evaluate a multimodal treatment of using STING agonists during the chronic persistent arthritic phase to reduce viral-induced inflammation and eliminate persistent infection. However, it is important to note that in chronic chikungunya disease, treatment with cAIMP may further aggravate joint inflammation. This potential adverse effect may limit cAIMP therapeutic efficacy at the chronic phase of disease. Moreover, utilization of well-dose-controlled treatment of cAIMP during chronic disease can promote effective humoral and cell-mediated immune response. This can result in sterilizing immunity by clearing virus from reservoir cells. The direct-acting antiviral (DAA) remdesivir exhibited selectivity against the tested viruses. It has been demonstrated that remdesivir is readily incorporated by SARS-CoV-2 RNA-dependent RNA polymerase (RdRp) into the newly synthesized RNA strand, resulting in RdRp stalling.⁷⁵ This mechanism is more likely to be conserved in EV-D68 and RSV, whereas remdesivir was not effective against CHIKV and WNV, possibly due to evolutionary divergence of mosquito-borne arboviral RdRp structure. Thus, targeting common host factors can provide broader protection. The compounds identified in this study can be further developed in combination with other antivirals to be potentially used in the event of respiratory and arboviral disease outbreaks.

Limitations of the study

We acknowledge some limitations of this study. First, the identified innate immune agonists including cAIMP exhibit antiviral activity and may have limited clinical application. Thus, more potent but safe synthetic derivatives need to be further developed and evaluated in preclinical and clinical studies. Second, activation of the immune system likely has unintended consequences of triggering autoimmune response; therefore, drug dose and treatment duration require further cautious optimization. Third, as we conducted animal efficacy experiments with single-dose treatment immediately after exposure to CHIKV (6 and 12 hpi), additional studies are warranted to evaluate cAIMP therapeutic potential in the chronic phase of CHIKV arthritis. Lastly, innate immune agonists have been used as

Figure 6. STING agonist cAIMP prophylactic and treatment measures mitigate CHIKV-mediated viral arthritis

- (A) Schematic diagram of timeline highlighting time of infection, administration of the compound, and tissue harvest.
- (B) Systemic administration of cAIMP induces the expression of antiviral genes. Graph shows the transcriptional activation of STING/type 1 IFN genes in the left footpad at 24 h after drug treatment (n = 5 mice/group). Student's t test. *p > 0.01.
- (C) Graphs show body weight, left footpad volume, and viral genome replication (left footpad at 3 dpi) of cAIMP-treated or vehicle-treated mice. cAIMP pre-treatment reduces foot swelling in CHIKV-infected (181/25) mice. Student's t test and a non-parametric t test (Mann-Whitney test) were used. **p > 0.001, ***p > 0.0001. n = 2 independent experiments.
- (D) Dot plot analysis of overrepresented up- or downregulated pathways in CHIKV-infected and cAIMP-treated/virus-infected left footpad of mice at 7 dpi are shown.
- (E) Histopathological analysis of CHIKV-infected left rear footpad at 7 dpi. Microscopic images of H&E staining of muscle, skin, and joint tissues are presented. Note: heavy inflammatory cell infiltration in the saline group. Saline group synovial cavity (asterisk) in the joint is filled with fibrinous exudate. C, cartilage; B, bone; S, synovial membrane. IHC images indicate infiltrating macrophages and T cells (dark brown) in the left footpad of vehicle- (saline) or cAIMP-treated mice at 7 dpi. Image magnification with 20× or 40× objective lens.
- (F) cAIMP drug treatment at 6 or 12 h post-CHIKV infection provides long-term therapeutic benefit by reducing footpad swelling CHIKV viral load (n = 5–6 mice). No significant body weight changes observed in any of the groups. Student's t test. *p > 0.01, **p > 0.001, ***p > 0.0001.
- See also [Figures S6](#) and [S7](#).

vaccine adjuvants to potentiate pathogen-specific antibody and cell-mediated immune responses, thus future studies need to be directed to test the efficiency of cAIMP in adaptive immune-mediated clearances of persistent CHIKV infection.

STAR★METHODS

Detailed methods are provided in the online version of this paper and include the following:

- **KEY RESOURCES TABLE**
- **RESOURCE AVAILABILITY**
 - Lead contact
 - Materials availability
 - Data and code availability
- **EXPERIMENTAL MODEL AND SUBJECT DETAILS**
 - Ethics statement
 - Cells
 - Viruses
 - *In vivo* mice experiment for CHIKV infection
- **METHOD DETAILS**
 - Drug library and compounds
 - Viral infection for drug testing
 - *Viral titer by TCID₅₀* (median tissue culture infectious dose) assay
 - Cell viability and ATP assay
 - NAD/NADH-Glo assay
 - Histopathology
 - Immunohistochemistry
 - Viral infection and RNA sample preparation for RNA sequencing analysis
 - RNA sequencing data analysis
 - Western blot analysis
- **QUANTIFICATION AND STATISTICAL ANALYSIS**
 - Image analysis/quantification
 - Statistics and data analysis

SUPPLEMENTAL INFORMATION

Supplemental information can be found online at <https://doi.org/10.1016/j.xcrm.2023.101024>.

ACKNOWLEDGMENTS

We are grateful to Barbara Dillon, UCLA High Containment Program Director, for BSL3 work. We thank Yijie Wang from the UCLA Cardiomyocyte Core for providing hPSC-CMs. This study is partly supported by National Institutes of Health awards 1R01EY032149-01, 5R01AI163216-02, and 1R01DK132735-01 to V.A. The viruses used in this study were obtained through BEI Resources, NIAID, NIH.

AUTHOR CONTRIBUTIONS

G.G.J. conducted conception and design, collection and/or assembly of data, data analysis and interpretation, and manuscript writing. J.I.I., A.V.J., S.D., C.C., S.C.C., N.P., S.A., A.S., A.L.M., and A.F. conducted and assisted with experiments and data analysis and interpretation. N.C., S.S., S.W.F., S.J., and M.S.P. assisted with experimental design, data analysis, data interpretation, and manuscript writing. A.R. conducted conception and design, bioinformatics data analysis and interpretation, and manuscript writing. V.A. conduct-

ed and provided conception and design, data analysis and interpretation, manuscript writing, and final approval of manuscript.

DECLARATION OF INTERESTS

The authors declare no competing interests.

Received: January 28, 2023

Revised: March 17, 2023

Accepted: April 7, 2023

Published: April 28, 2023

REFERENCES

1. Constant, L.E.C., Rajsufus, B.F., Carneiro, P.H., Sisnande, T., Mohana-Borges, R., and Allonso, D. (2021). Overview on chikungunya virus infection: from epidemiology to state-of-the-art experimental models. *Front. Microbiol.* *12*, 744164. <https://doi.org/10.3389/fmicb.2021.744164>.
2. Musso, D., Rodriguez-Morales, A.J., Levi, J.E., Cao-Lormeau, V.-M., and Gubler, D.J. (2018). Unexpected outbreaks of arbovirus infections: lessons learned from the Pacific and tropical America. *Lancet Infect. Dis.* *18*, e355–e361. [https://doi.org/10.1016/S1473-3099\(18\)30269-X](https://doi.org/10.1016/S1473-3099(18)30269-X).
3. Gould, E., Pettersson, J., Higgs, S., Charrel, R., and de Lamballerie, X. (2017). Emerging arboviruses: why today? *One Health* *4*, 1–13. <https://doi.org/10.1016/j.onehlt.2017.06.001>.
4. Ozden, S., Huerre, M., Riviere, J.P., Coffey, L.L., Afonso, P.V., Mouly, V., de Monredon, J., Roger, J.C., El Amrani, M., Yin, J.L., et al. (2007). Human muscle satellite cells as targets of Chikungunya virus infection. *PLoS One* *2*, e527. <https://doi.org/10.1371/journal.pone.0000527>.
5. Martins, H.A., Bernardino, S.N., Santos, C.C., and Ribas, V.R. (2016). Chikungunya and myositis: a case report in Brazil. *J. Clin. Diagn. Res.* *10*, OD05–OD06. <https://doi.org/10.7860/JCDR/2016/23680.9053>.
6. Alvarez, M.F., Bolivar-Mejia, A., Rodriguez-Morales, A.J., and Ramirez-Vallejo, E. (2017). Cardiovascular involvement and manifestations of systemic Chikungunya virus infection: a systematic review. *F1000Res.* *6*, 390. <https://doi.org/10.12688/f1000research.11078.2>.
7. Brasil, P., Pereira, J.P., Moreira, M.E., Ribeiro Nogueira, R.M., Damasceno, L., Wakimoto, M., Rabello, R.S., Valderramos, S.G., Halai, U.-A., Salles, T.S., et al. (2016). Zika virus infection in pregnant women in Rio de Janeiro. *N. Engl. J. Med.* *375*, 2321–2334. <https://doi.org/10.1056/NEJMoa1602412>.
8. Cranston, J.S., Tiene, S.F., Nielsen-Saines, K., Vasconcelos, Z., Pone, M.V., Pone, S., Zin, A., Salles, T.S., Pereira, J.P., Jr., Orofino, D., et al. (2020). Association between antenatal exposure to Zika virus and anatomical and neurodevelopmental abnormalities in children. *JAMA Netw. Open* *3*, e209303. <https://doi.org/10.1001/jamanetworkopen.2020.9303>.
9. Petersen, L.R., Brault, A.C., and Nasci, R.S. (2013). West Nile virus: review of the literature. *JAMA* *310*, 308–315. <https://doi.org/10.1001/jama.2013.8042>.
10. DeBiasi, R.L., and Tyler, K.L. (2006). West Nile virus meningoencephalitis. *Nat. Clin. Pract. Neurol.* *2*, 264–275. <https://doi.org/10.1038/ncpneuro0176>.
11. Shi, J., Su, Z., Fan, Z., Wang, J., Liu, S., Zhang, B., Wei, H., Jehan, S., Jamil, N., Shen, S., and Deng, F. (2017). Extensive evolution analysis of the global chikungunya virus strains revealed the origination of CHIKV epidemics in Pakistan in 2016. *Viol. Sin.* *32*, 520–532. <https://doi.org/10.1007/s12250-017-4077-5>.
12. Phadungsombath, J., Imad, H.A., Nakayama, E.E., Leaugwutiwong, P., Ramasoota, P., Nguitragool, W., Matsee, W., Piyaphanee, W., and Shioda, T. (2022). Spread of a novel Indian Ocean Lineage carrying E1-K211e/E2-V264A of chikungunya virus east/central/South African genotype across the Indian subcontinent, Southeast Asia, and eastern Africa. *Microorganisms* *10*, 354. <https://doi.org/10.3390/microorganisms10020354>.
13. Translational Research Consortia for Chikungunya Virus in, I. (2021). Current status of chikungunya in India. *Front. Microbiol.* *12*, 695173. <https://doi.org/10.3389/fmicb.2021.695173>.

14. Khongwicht, S., Chansaenroj, J., Thongmee, T., Benjamanukul, S., Wanlapakorn, N., Chirathaworn, C., and Poovorawan, Y. (2021). Large-scale outbreak of Chikungunya virus infection in Thailand, 2018–2019. *PLoS One* *16*, e0247314. <https://doi.org/10.1371/journal.pone.0247314>.
15. Cunha, M.S., Costa, P.A.G., Correa, I.A., de Souza, M.R.M., Calil, P.T., da Silva, G.P.D., Costa, S.M., Fonseca, V.W.P., and da Costa, L.J. (2020). Chikungunya virus: an emergent arbovirus to the South American continent and a continuous threat to the world. *Front. Microbiol.* *11*, 1297. <https://doi.org/10.3389/fmicb.2020.01297>.
16. Gubler, D.J., Vasilakis, N., and Musso, D. (2017). History and emergence of Zika virus. *J. Infect. Dis.* *216*, S860–S867. <https://doi.org/10.1093/infdis/jix451>.
17. Bakhshi, H., Mousson, L., Moutailler, S., Vazeille, M., Piorkowski, G., Zakeri, S., Raz, A., de Lamballerie, X., Dinparast-Djadid, N., and Failloux, A.B. (2020). Detection of arboviruses in mosquitoes: evidence of circulation of chikungunya virus in Iran. *PLoS Negl. Trop. Dis.* *14*, e0008135. <https://doi.org/10.1371/journal.pntd.0008135>.
18. Paz, S. (2015). Climate change impacts on West Nile virus transmission in a global context. *Phil. Trans. R. Soc. B.* *370*, 20130561. <https://doi.org/10.1098/rstb.2013.0561>.
19. Takeuchi, O., and Akira, S. (2010). Pattern recognition receptors and inflammation. *Cell* *140*, 805–820. <https://doi.org/10.1016/j.cell.2010.01.022>.
20. Choe, J., Kelker, M.S., and Wilson, I.A. (2005). Crystal structure of human toll-like receptor 3 (TLR3) ectodomain. *Science* *309*, 581–585. <https://doi.org/10.1126/science.1115253>.
21. Liu, L., Botos, I., Wang, Y., Leonard, J.N., Shiloach, J., Segal, D.M., and Davies, D.R. (2008). Structural basis of toll-like receptor 3 signaling with double-stranded RNA. *Science* *320*, 379–381. <https://doi.org/10.1126/science.1155406>.
22. Inohara, C., McDonald, C., McDonald, C., and Nuñez, G. (2005). NOD-LRR proteins: role in host-microbial interactions and inflammatory disease. *Annu. Rev. Biochem.* *74*, 355–383. <https://doi.org/10.1146/annurev-biochem.74.082803.133347>.
23. Brown, G.D. (2006). Dectin-1: a signalling non-TLR pattern-recognition receptor. *Nat. Rev. Immunol.* *6*, 33–43. <https://doi.org/10.1038/nri1745>.
24. Takeuchi, O., and Akira, S. (2009). Innate immunity to virus infection. *Immunol. Rev.* *227*, 75–86. <https://doi.org/10.1111/j.1600-065X.2008.00737.x>.
25. Yoneyama, M., and Fujita, T. (2008). Structural mechanism of RNA recognition by the RIG-I-like receptors. *Immunity* *29*, 178–181. <https://doi.org/10.1016/j.immuni.2008.07.009>.
26. Olagnier, D., Scholte, F.E.M., Chiang, C., Albucescu, I.C., Nichols, C., He, Z., Lin, R., Snijder, E.J., van Hemert, M.J., and Hiscott, J. (2014). Inhibition of dengue and chikungunya virus infections by RIG-I-mediated type I interferon-independent stimulation of the innate antiviral response. *J. Virol.* *88*, 4180–4194. <https://doi.org/10.1128/JVI.03114-13>.
27. Schroder, K., and Tschopp, J. (2010). The inflammasomes. *Cell* *140*, 821–832. <https://doi.org/10.1016/j.cell.2010.01.040>.
28. Geijtenbeek, T.B.H., and Gringhuis, S.I. (2009). Signalling through C-type lectin receptors: shaping immune responses. *Nat. Rev. Immunol.* *9*, 465–479. <https://doi.org/10.1038/nri2569>.
29. Motwani, M., Pesiridis, S., and Fitzgerald, K.A. (2019). DNA sensing by the cGAS–STING pathway in health and disease. *Nat. Rev. Genet.* *20*, 657–674. <https://doi.org/10.1038/s41576-019-0151-1>.
30. Cai, X., Chiu, Y.-H., and Chen, Z.J. (2014). The cGAS–cGAMP–STING pathway of cytosolic DNA sensing and signaling. *Mol. Cell* *54*, 289–296. <https://doi.org/10.1016/j.molcel.2014.03.040>.
31. Miyake, K., Shibata, T., Ohto, U., Shimizu, T., Saitoh, S.-I., Fukui, R., and Murakami, Y. (2018). Mechanisms controlling nucleic acid-sensing Toll-like receptors. *Int. Immunol.* *30*, 43–51. <https://doi.org/10.1093/intimm/dxy016>.
32. Chen, J., Gao, X.M., Zhao, H., Cai, H., Zhang, L., Cao, X.X., Zhou, D.B., and Li, J. (2021). A highly heterogeneous mutational pattern in POEMS syndrome. *Leukemia* *35*, 1100–1107. <https://doi.org/10.1038/s41375-020-01101-4>.
33. Sooksawasdi Na Ayudhya, S., Laksono, B.M., and van Riel, D. (2021). The pathogenesis and virulence of enterovirus-D68 infection. *Virulence* *12*, 2060–2072. <https://doi.org/10.1080/21505594.2021.1960106>.
34. Kushawaha, A., Jadonath, S., and Mobarakai, N. (2009). West Nile virus myocarditis causing a fatal arrhythmia: a case report. *Cases J.* *2*, 7147. <https://doi.org/10.1186/1757-1626-2-7147>.
35. Shah, K.S., Hale Hammond, M.E., Drakos, S.G., Anderson, J.L., Fang, J.C., Knowlton, K.U., and Shaw, R.M. (2021). SARS-CoV-2 as an inflammatory cardiovascular disease: current knowledge and future challenges. *Future Cardiol.* *17*, 1277–1291. <https://doi.org/10.2217/fca-2020-0188>.
36. Madjid, M., Safavi-Naeini, P., Solomon, S.D., and Vardeny, O. (2020). Potential effects of coronaviruses on the cardiovascular system: a review. *JAMA Cardiol.* *5*, 831–840. <https://doi.org/10.1001/jamacardio.2020.1286>.
37. Peiris, J.S.M., Chu, C.M., Cheng, V.C.C., Chan, K.S., Hung, I.F.N., Poon, L.L.M., Law, K.I., Tang, B.S.F., Hon, T.Y.W., Chan, C.S., et al. (2003). Clinical progression and viral load in a community outbreak of coronavirus-associated SARS pneumonia: a prospective study. *Lancet* *361*, 1767–1772. [https://doi.org/10.1016/s0140-6736\(03\)13412-5](https://doi.org/10.1016/s0140-6736(03)13412-5).
38. Sharma, A., Garcia, G., Jr., Wang, Y., Plummer, J.T., Morizono, K., Arumugaswami, V., and Svendsen, C.N. (2020). Human iPSC-derived cardiomyocytes are susceptible to SARS-CoV-2 infection. *Cell Rep. Med.* *1*, 100052. <https://doi.org/10.1016/j.xcrm.2020.100052>.
39. Garcia, G., Jr., Jeyachandran, A.V., Wang, Y., Irudayam, J.I., Cario, S.C., Sen, C., Li, S., Li, Y., Kumar, A., Nielsen-Saines, K., et al. (2022). Hippo signaling pathway activation during SARS-CoV-2 infection contributes to host antiviral response. *PLoS Biol.* *20*, e3001851. <https://doi.org/10.1371/journal.pbio.3001851>.
40. Garcia, G., Jr., Sharma, A., Ramaiah, A., Sen, C., Purkayastha, A., Kohn, D.B., Parcells, M.S., Beck, S., Kim, H., Bakowski, M.A., et al. (2021). Antiviral drug screen identifies DNA-damage response inhibitor as potent blocker of SARS-CoV-2 replication. *Cell Rep.* *35*, 108940. <https://doi.org/10.1016/j.celrep.2021.108940>.
41. Morrison, T.E., Oko, L., Montgomery, S.A., Whitmore, A.C., Lotstein, A.R., Gunn, B.M., Elmore, S.A., and Heise, M.T. (2011). A mouse model of chikungunya virus-induced musculoskeletal inflammatory disease: evidence of arthritis, tenosynovitis, myositis, and persistence. *Am. J. Pathol.* *178*, 32–40. <https://doi.org/10.1016/j.ajpath.2010.11.018>.
42. Hawman, D.W., Stoermer, K.A., Montgomery, S.A., Pal, P., Oko, L., Diamond, M.S., and Morrison, T.E. (2013). Chronic joint disease caused by persistent Chikungunya virus infection is controlled by the adaptive immune response. *J. Virol.* *87*, 13878–13888. <https://doi.org/10.1128/jvi.02666-13>.
43. Geng, T., Lin, T., Yang, D., Harrison, A.G., Vella, A.T., Fikrig, E., and Wang, P. (2021). A critical role for STING signaling in limiting pathogenesis of chikungunya virus. *J. Infect. Dis.* *223*, 2186–2196. <https://doi.org/10.1093/infdis/jiaa694>.
44. Nazmi, A., Mukhopadhyay, R., Dutta, K., and Basu, A. (2012). STING mediates neuronal innate immune response following Japanese encephalitis virus infection. *Sci. Rep.* *2*, 347. <https://doi.org/10.1038/srep00347>.
45. You, F., Wang, P., Yang, L., Yang, G., Zhao, Y.O., Qian, F., Walker, W., Sutton, R., Montgomery, R., Lin, R., et al. (2013). ELF4 is critical for induction of type I interferon and the host antiviral response. *Nat. Immunol.* *14*, 1237–1246.
46. Chen, H., Sun, H., You, F., Sun, W., Zhou, X., Chen, L., Yang, J., Wang, Y., Tang, H., Guan, Y., et al. (2011). Activation of STAT6 by STING is critical for antiviral innate immunity. *Cell* *147*, 436–446. <https://doi.org/10.1016/j.cell.2011.09.022>.
47. Ishikawa, H., Ma, Z., and Barber, G.N. (2009). STING regulates intracellular DNA-mediated, type I interferon-dependent innate immunity. *Nature* *461*, 788–792. <https://doi.org/10.1038/nature08476>.
48. Willemsen, J., Neuheff, M.T., Hoyle, T., Noir, E., Tessier, C., Sarret, S., Thorsen, T.N., Littlewood-Evans, A., Zhang, J., Hasan, M., et al. (2021). TNF leads to mtDNA release and cGAS/STING-dependent interferon

- responses that support inflammatory arthritis. *Cell Rep.* 37, 109977. <https://doi.org/10.1016/j.celrep.2021.109977>.
49. Cheng, W.Y., He, X.B., Jia, H.J., Chen, G.H., Jin, Q.W., Long, Z.L., and Jing, Z.Z. (2018). The cGas-sting signaling pathway is required for the innate immune response against ectromelia virus. *Front. Immunol.* 9, 1297. <https://doi.org/10.3389/fimmu.2018.01297>.
 50. Slavik, K.M., Morehouse, B.R., Ragucci, A.E., Zhou, W., Ai, X., Chen, Y., Li, L., Wei, Z., Bähre, R., König, M., et al. (2021). cGAS-like receptors sense RNA and control 3'2'-cGAMP signalling in *Drosophila*. *Nature* 597, 109–113. <https://doi.org/10.1038/s41586-021-03743-5>.
 51. Webb, L.G., Veloz, J., Pintado-Silva, J., Zhu, T., Rangel, M.V., Mutetwa, T., Zhang, L., Bernal-Rubio, D., Figueroa, D., Carrau, L., et al. (2020). Chikungunya virus antagonizes cGAS-STING mediated type-I interferon responses by degrading cGAS. *PLoS Pathog.* 16, e1008999. <https://doi.org/10.1371/journal.ppat.1008999>.
 52. Gall, B., Pryke, K., Abraham, J., Mizuno, N., Botto, S., Sali, T.M., Broeckel, R., Haese, N., Nilsen, A., Placzek, A., et al. (2018). Emerging alphaviruses are sensitive to cellular States induced by a novel small-molecule agonist of the STING pathway. *J. Virol.* 92, e01913-17. <https://doi.org/10.1128/JVI.01913-17>.
 53. Sali, T.M., Pryke, K.M., Abraham, J., Liu, A., Archer, I., Broeckel, R., Stavrosky, J.A., Smith, J.L., Al-Shammari, A., Amsler, L., et al. (2015). Characterization of a novel human-specific STING agonist that elicits antiviral activity against emerging alphaviruses. *PLoS Pathog.* 11, e1005324. <https://doi.org/10.1371/journal.ppat.1005324>.
 54. Schoggins, J.W., MacDuff, D.A., Imanaka, N., Gainey, M.D., Shrestha, B., Eitson, J.L., Mar, K.B., Richardson, R.B., Ratushny, A.V., Litvak, V., et al. (2014). Pan-viral specificity of IFN-induced genes reveals new roles for cGAS in innate immunity. *Nature* 505, 691–695. <https://doi.org/10.1038/nature12862>.
 55. Ahola, T., Lampio, A., Auvinen, P., and Kääriäinen, L. (1999). Semliki Forest virus mRNA capping enzyme requires association with anionic membrane phospholipids for activity. *EMBO J.* 18, 3164–3172. <https://doi.org/10.1093/emboj/18.11.3164>.
 56. Kumar, S., Kumar, A., Mamidi, P., Tiwari, A., Kumar, S., Mayavannan, A., Mudulli, S., Singh, A.K., Subudhi, B.B., and Chattopadhyay, S. (2018). Chikungunya virus nsP1 interacts directly with nsP2 and modulates its ATPase activity. *Sci. Rep.* 8, 1045. <https://doi.org/10.1038/s41598-018-19295-0>.
 57. Lampio, A., Kilpeläinen, I., Pesonen, S., Karhi, K., Auvinen, P., Somerharju, P., and Kääriäinen, L. (2000). Membrane binding mechanism of an RNA virus-capping enzyme. *J. Biol. Chem.* 275, 37853–37859. <https://doi.org/10.1074/jbc.M004865200>.
 58. Yu, L., and Liu, P. (2021). Cytosolic DNA sensing by cGAS: regulation, function, and human diseases. *Signal Transduct. Target. Ther.* 6, 170. <https://doi.org/10.1038/s41392-021-00554-y>.
 59. de Groot, R.J., Rümenapf, T., Kuhn, R.J., Strauss, E.G., and Strauss, J.H. (1991). Sindbis virus RNA polymerase is degraded by the N-end rule pathway. *Proc. Natl. Acad. Sci. USA* 88, 8967–8971. <https://doi.org/10.1073/pnas.88.20.8967>.
 60. Li, M., Ferretti, M., Ying, B., Descamps, H., Lee, E., Dittmar, M., Lee, J.S., Whig, K., Kamalia, B., Dohnalová, L., et al. (2021). Pharmacological activation of STING blocks SARS-CoV-2 infection. *Sci. Immunol.* 6, eabi9007. <https://doi.org/10.1126/sciimmunol.abi9007>.
 61. Van Herck, S., Feng, B., and Tang, L. (2021). Delivery of STING agonists for adjuvanting subunit vaccines. *Adv. Drug Deliv. Rev.* 179, 114020. <https://doi.org/10.1016/j.addr.2021.114020>.
 62. Le Naour, J., Zitvogel, L., Galluzzi, L., Vacchelli, E., and Kroemer, G. (2020). Trial watch: STING agonists in cancer therapy. *Oncoimmunology* 9, 1777624. <https://doi.org/10.1080/2162402X.2020.1777624>.
 63. Ishikawa, H., and Barber, G.N. (2008). STING is an endoplasmic reticulum adaptor that facilitates innate immune signalling. *Nature* 455, 674–678. <https://doi.org/10.1038/nature07317>.
 64. Li, X.D., Wu, J., Gao, D., Wang, H., Sun, L., and Chen, Z.J. (2013). Pivotal roles of cGAS-cGAMP signaling in antiviral defense and immune adjuvant effects. *Science* 341, 1390–1394. <https://doi.org/10.1126/science.1244404>.
 65. Barber, G.N. (2015). STING: infection, inflammation and cancer. *Nat. Rev. Immunol.* 15, 760–770. <https://doi.org/10.1038/nri3921>.
 66. Gao, D., Wu, J., Wu, Y.T., Du, F., Aroh, C., Yan, N., Sun, L., and Chen, Z.J. (2013). Cyclic GMP-AMP synthase is an innate immune sensor of HIV and other retroviruses. *Science* 341, 903–906. <https://doi.org/10.1126/science.1240933>.
 67. Goertz, G.P., Vogels, C.B.F., Geertsema, C., Koenraadt, C.J.M., and Pijlman, G.P. (2017). Mosquito co-infection with Zika and chikungunya virus allows simultaneous transmission without affecting vector competence of *Aedes aegypti*. *PLoS Negl. Trop. Dis.* 11, e0005654. <https://doi.org/10.1371/journal.pntd.0005654>.
 68. Zaidi, M.B., Garcia-Cordero, J., Rivero-Gomez, R., Corzo-Gomez, J., González Y Almeida, M.E., Bonilla-Moreno, R., Bustos-Arriaga, J., Villegas-Sepulveda, N., Flores-Romo, L., and Cedillo-Barron, L. (2018). Competitive suppression of dengue virus replication occurs in chikungunya and dengue co-infected Mexican infants. *Parasit. Vectors* 11, 378. <https://doi.org/10.1186/s13071-018-2942-1>.
 69. Chusri, S., Siripaitoon, P., Silpapojakul, K., Hortiwakul, T., Charernmak, B., Chinnawirotpisan, P., Nisalak, A., Thaisomboonsuk, B., Klungthong, C., Gibbons, R.V., and Jarman, R.G. (2014). Kinetics of chikungunya virus infections during an outbreak in Southern Thailand, 2008–2009. *Am. J. Trop. Med. Hyg.* 90, 410–417. <https://doi.org/10.4269/ajtmh.12-0681>.
 70. Sudeep, A.B., Vyas, P.B., Parashar, D., and Shil, P. (2019). Differential susceptibility & replication potential of Vero E6, BHK-21, RD, A-549, C6/36 cells & *Aedes aegypti* mosquitoes to three strains of chikungunya virus. *Indian J. Med. Res.* 149, 771–777. https://doi.org/10.4103/ijmr.IJMR_453_17.
 71. Esposito, S., Salice, P., Bosis, S., Ghiglia, S., Tremolati, E., Tagliabue, C., Gualtieri, L., Barbier, P., Galeone, C., Marchisio, P., and Principi, N. (2010). Altered cardiac rhythm in infants with bronchiolitis and respiratory syncytial virus infection. *BMC Infect. Dis.* 10, 305. <https://doi.org/10.1186/1471-2334-10-305>.
 72. Couderc, T., Chrétien, F., Schilte, C., Disson, O., Brigitte, M., Guivel-Benhassine, F., Touret, Y., Barau, G., Cayet, N., Schuffenecker, I., et al. (2008). A mouse model for Chikungunya: young age and inefficient type-I interferon signaling are risk factors for severe disease. *PLoS Pathog.* 4, e29. <https://doi.org/10.1371/journal.ppat.0040029>.
 73. Haese, N.N., Broeckel, R.M., Hawman, D.W., Heise, M.T., Morrison, T.E., and Streblow, D.N. (2016). Animal models of chikungunya virus infection and disease. *J. Infect. Dis.* 214, S482–S487. <https://doi.org/10.1093/infdis/jiw284>.
 74. Rudd, P.A., Wilson, J., Gardner, J., Larcher, T., Babarit, C., Le, T.T., Anraku, I., Kumagai, Y., Loo, Y.M., Gale, M., Jr., et al. (2012). Interferon response factors 3 and 7 protect against Chikungunya virus hemorrhagic fever and shock. *J. Virol.* 86, 9888–9898. <https://doi.org/10.1128/jvi.00956-12>.
 75. Kocic, G., Hillen, H.S., Tegunov, D., Dienemann, C., Seitz, F., Schmitzova, J., Farnung, L., Siewert, A., Höbartner, C., and Cramer, P. (2021). Mechanism of SARS-CoV-2 polymerase stalling by remdesivir. *Nat. Commun.* 12, 279. <https://doi.org/10.1038/s41467-020-20542-0>.
 76. Lian, X., Hsiao, C., Wilson, G., Zhu, K., Hazeltine, L.B., Azarin, S.M., Raval, K.K., Zhang, J., Kamp, T.J., and Palecek, S.P. (2012). Robust cardiomyocyte differentiation from human pluripotent stem cells via temporal modulation of canonical Wnt signaling. *Proc. Natl. Acad. Sci. USA* 109, E1848–E1857. <https://doi.org/10.1073/pnas.1200250109>.
 77. Dobin, A., Davis, C.A., Schlesinger, F., Drenkow, J., Zaleski, C., Jha, S., Batut, P., Chaisson, M., and Gingeras, T.R. (2013). STAR: ultrafast universal RNA-seq aligner. *Bioinformatics* 29, 15–21. <https://doi.org/10.1093/bioinformatics/bts635>.
 78. Love, M.I., Huber, W., and Anders, S. (2014). Moderated estimation of fold change and dispersion for RNA-seq data with DESeq2. *Genome Biol.* 15, 550. <https://doi.org/10.1186/s13059-014-0550-8>.

79. Jassal, B., Matthews, L., Viteri, G., Gong, C., Lorente, P., Fabregat, A., Sidiropoulos, K., Cook, J., Gillespie, M., Haw, R., et al. (2020). The reactome pathway knowledgebase. *Nucleic Acids Res.* 48, D498–d503. <https://doi.org/10.1093/nar/gkz1031>.
80. Gauger, P.C., and Vincent, A.L. (2014). Serum virus neutralization assay for detection and quantitation of serum-neutralizing antibodies to influenza A virus in swine. *Methods in molecular biology. Methods Mol. Biol.* 1161, 313–324. https://doi.org/10.1007/978-1-4939-0758-8_26.
81. Partek-Inc (2020). Partek® Flow® (Version 10.0) [Computer Software].
82. Mi, H., Ebert, D., Muruganujan, A., Mills, C., Albu, L.P., Mushayamaha, T., and Thomas, P.D. (2021). PANTHER version 16: a revised family classification, tree-based classification tool, enhancer regions and extensive API. *Nucleic Acids Res.* 49, D394–D394. <https://doi.org/10.1093/nar/gkaa1106>.
83. Mi, H., Muruganujan, A., Ebert, D., Huang, X., and Thomas, P.D. (2019). PANTHER version 14: more genomes, a new PANTHER GO-slim and improvements in enrichment analysis tools. *Nucleic Acids Res.* 47, D419–D426. <https://doi.org/10.1093/nar/gky1038>.

STAR★METHODS

KEY RESOURCES TABLE

REAGENT or RESOURCE	SOURCE	IDENTIFIER
Antibodies		
Anti-CHIKV E2 Antibody, clone 1.3A2	MilliporeSigma	Cat#MABF2007
Chikungunya virus nsP3 antibody	Genetex	Cat#GTX135189
Anti-Chikungunya virus (CHIKV) [11E7] Antibody	Kerafast	Cat#ESG001
Flavivirus group antibody [D1-4G2-4-15 (4G2)]	Genetex	Cat#GTX57154; RRID: AB_2887950
Enterovirus D68 VP1 antibody	Genetex	Cat#GTX132313
Respiratory Syncytial virus antibody [BDI065]	Genetex	Cat#GTX44267
Monoclonal anti-SARS-CoV S protein (Similar to 240C) antibody	BEI Resources Repository	Cat#NR-616
TBK1/NAK (D1B4)	Cell Signaling Technology	Cat#3504S; RRID: AB_2255663
Phospho-TBK1/NAK (Ser172)	Cell Signaling Technology	Cat#5483S; RRID: AB_10693472
Anti-IRF3 (phospho S386) antibody [EPR2346] (ab76493)	Abcam	Cat#ab76493; RRID: AB_1523836
IRF-3 (D6I4C) XP® Rabbit mAb	Cell Signaling Technology	Cat#11904S; RRID: AB_2722521
Phospho-Stat1 (Tyr701) (58D6) Rabbit mAb	Cell Signaling Technology	Cat#9167S; RRID: AB_561284
Stat1 (D1K9Y) Rabbit mAb	Cell Signaling Technology	Cat#14994; RRID: AB_2737027
Phospho-STING (Ser366) (D7C3S) Rabbit mAb	Cell Signaling Technology	Cat#19781S; RRID: AB_2737062
STING (D2P2F) Rabbit mAb #13647	Cell Signaling Technology	Cat#13647; RRID: AB_2732796
NF-κB p65 (D14E12) Rabbit mAb	Cell Signaling Technology	Cat#8242T; RRID: AB_10859369
Cleaved caspase-3 rabbit monoclonal antibody, clone D175	Cell Signaling Technology	Cat#9661S; RRID: AB_2341188
Goat anti-Mouse IgG (H + L) Cross-Adsorbed Secondary Antibody, Alexa Fluor 555	Thermo Fisher Scientific	Cat#A21422; RRID: AB_141822
IgG (H + L) Cross-Adsorbed Goat anti-Rabbit, Alexa Fluor 488, Invitrogen	Thermo Fisher Scientific	Cat#A11008; RRID: AB_143165
Goat anti-Guinea Pig IgG (H + L) Highly Cross-Adsorbed Secondary Antibody, Alexa Fluor 488	Thermo Fisher Scientific	Cat#A11073; RRID: AB_2534117
Monoclonal Anti-Beta-Actin, Clone AC-74 produced in mouse	MilliporeSigma	Cat#A2228; RRID: AB_476697
Bacterial and virus strains		
SARS-Related Coronavirus 2 (SARS-CoV-2), Isolate USA-WA1/2020	BEI Resources Repository	Cat#NR-52281
Chikungunya virus (CHIKV), H 20235-St. Martin-2013	BEI Resources Repository	Cat#NR-49901
Chikungunya virus (CHIKV), 181/25	BEI Resources Repository	Cat#NR-13222
West Nile Virus, 385-99	BEI Resources Repository	Cat#NR-158
Enterovirus D68 – USA/2018-23087	BEI Resources Repository	Cat#NR-52015
Human Respiratory Syncytial Virus – A2000/3-4	BEI Resources Repository	Cat# NR-28530
Human respiratory syncytial virus – A2001/3-12	BEI Resources Repository	Cat# NR-28526
Zika virus (ZIKV), PRVABC59	ATCC	Cat#VR-1843
Chemicals, peptides, and recombinant proteins		
Regular Fetal Bovine Serum	Corning	Cat#35010CV
Eagle's Minimum Essential Medium (MEM)	Corning	Cat#10009CV
Penicillin-Streptomycin (10,000 U/mL)	Gibco	Cat#15140122
L-Glutamine (200 mM)	Gibco	Cat#25030081
diABZI STING agonist	Selleckchem	Cat#S8796

(Continued on next page)

Continued

REAGENT or RESOURCE	SOURCE	IDENTIFIER
2'3'-cGAMP	Invivogen	Cat#tlrl-nacga23
3'3'-cGAMP	Invivogen	Cat#tlrl-nacga
Adilipoline™ (CL413)	Invivogen	Cat#tlrl-c413
C12-iE-DAP	Invivogen	Cat#tlrl-c12dap
cAIMP	Invivogen	Cat#tlrl-nacai
c-di-AMP	Invivogen	Cat#tlrl-nacda
c-di-GMP	Invivogen	Cat#tlrl-nacdg
FLA-BS	Invivogen	Cat#tlrl-bsfla
FSL-1	Invivogen	Cat#tlrl-fsl
Gardiquimod	Invivogen	Cat#tlrl-gdqs
iE-DAP	Invivogen	Cat#tlrl-dap
Imiquimod	Invivogen	Cat#tlrl-imqs
Loxoribine	Invivogen	Cat#tlrl-lox
LPS-RS	Invivogen	Cat#tlrl-rslps
LTA-BS	Invivogen	Cat#tlrl-lta
MDP	Invivogen	Cat#tlrl-mdp
ODN 4084-F	Invivogen	Cat#tlrl-4084
Pam2CSK4	Invivogen	Cat#tlrl-pm2s-1
Pam3CSK4	Invivogen	Cat#tlrl-pms
Poly(A:U)	Invivogen	Cat#tlrl-pau
Poly(dA:dT) naked	Invivogen	Cat#tlrl-patn
Poly(dG:dC) naked	Invivogen	Cat#tlrl-pgcn
Poly(I:C) (HMW)	Invivogen	Cat#tlrl-pic
Poly(I:C) (LMW)	Invivogen	Cat#tlrl-picw
Scleroglucan	Invivogen	Cat#tlrl-scg
TL8-506	Invivogen	Cat#tlrl-tl8506
Recombinant Human IFN-β	Peptotech	Cat#300-02BC
Remdesivir (GS-5734)	Selleckchem	Cat#S8932
6-Azauridine	MilliporeSigma	Cat#A1882
Dimethyl sulfoxide	MilliporeSigma	Cat#D2650
RPMI 1640	Thermo Fisher Scientific	Cat#11875093
B27 supplement with insulin	Thermo Fisher Scientific	Cat#17504044
CHIR-99021 (CT99021)	Selleckchem	Cat#S1263
IWR-1	MilliporeSigma	Cat#I0161
Methanol (Histological)	Thermo Fisher Scientific	Cat#A433P4
16% Paraformaldehyde (formaldehyde) aqueous solution	Electron Microscopy Sciences	Cat#15710
Dulbecco's Phosphate-Buffered Salt Solution 1X	Corning	Cat#21030CV
DAPI (4',6-Diamidino-2-Phenylindole, Dihydrochloride)	Thermo Fisher Scientific	Cat#D1306
Corning™ Cell Culture Phosphate Buffered Saline (1X)	Thermo Fisher Scientific	Cat#MT21040CV
Bovine Serum Albumin	MilliporeSigma	Cat#A9418
Normal Donkey Serum	Jackson ImmunoResearch	Cat#017-000-121
Normal Goat Serum	Cell Signaling Technology	Cat#5425S
Triton X-100	MilliporeSigma	Cat#T9284
Critical commercial assays		
CellTiter-Glo Luminescent Cell Viability Assay	Promega	Cat#G7570
NAD/NADH-Glo™ and NADP/NADPH-Glo™ Assays	Promega	Cat#G9071

(Continued on next page)

Continued

REAGENT or RESOURCE	SOURCE	IDENTIFIER
Deposited data		
RNA-Seq of mice or HFF-1 cells infected with CHIKV and/or treated with cAIMP or Scleroglucan	Gene Expression Omnibus	Accession Number: GSE197744
Experimental models: Cell lines		
VERO C1008 [Vero 76, clone E6, Vero E6]	ATCC	Cat#CRL-158
HFF-1 Cells	ATCC	Cat#SCRC-1041
A549 Cells	ATCC	Cat#CCL-185
hPSC derived cardiomyocyte	University of California, Los Angeles (Li et al. ⁶⁰)	N/A
Rhabdomyosarcoma (RD) cells	ATCC	Cat#CCL-136
Experimental Models: <i>In Vivo</i>		
C57BL/6J	UCLA	N/A
Oligonucleotides		
Primers for CHIKV (Forward:GATCCGGACTCAACCATCCT; Reverse:CATCGGGCAAACGCAGTGTA)	This Paper	N/A
Primers for ZIKV (Forward:AAGTACACATACCAAACAAAGTGGT; Reverse:TCCGCTCCCCCTTTGGTCTTG)	This Paper	N/A
Primers for WNV (Forward:CGGAAGTYGRGTAKACGGTGCTG; Reverse:CGGTWYTGAGGGCTTACRTGG)	Vázquez ¹	https://doi.org/10.1016/j.jviromet.2016.07.026
Primers for Human TRIM21 (Forward: CCAATCCGTGGCTGATACTT; Reverse: ACCCAGGACCATAGGATAACT)	This Paper	N/A
Primers for Human OAS2 (Forward:CATAGACCCTCAGGAGAGAAGA; Reverse:TCCAAAGACAATCAGGGTATGG)	This Paper	N/A
Primers for Human IFI44L (Forward:CACCCACCATCTACCTCAATAAA; Reverse:GCACACAGGAAGCAAGACTA)	This Paper	N/A
Primers for Human cGAS (Forward:TGTGGATATAACCCTGGCTTTG; Reverse:GCTTTAGTCGTAGTTGCTTCT)	This Paper	N/A
Primers for Human IFI16 (Forward:CCTGGAGGTATATCCTTTACAC; Reverse:GAGTTACGCTGGCACTTCTAA)	This Paper	N/A
Primers for Human STAT6 (Forward:GTTATGTCCAGCTACCATCAA; Reverse: GGGCCATTCCAAGGTCATAA)	This Paper	N/A
Primers for Mouse Oas1 (Forward: AGAGATGCTTCCAAGGTGC; Reverse: CTGATCCTCAAAGCTGGTGA)	This Paper	N/A
Primers for Mouse Trim21 (Forward:GATAGCCCAGAATACCAAGAAGAG; Reverse:GCCCATCTTCTCACAGAATAG)	This Paper	N/A
Primers for Mouse Ccl2 (Forward: AGTAGGCTGGAGAGCTACAA; Reverse:GTATGTCTGGACCATTCCTTC)	This Paper	N/A
Primers for Mouse Il-10 (Forward:CCCTTTGCTATGGTGCCTTTC; Reverse:AGGATCTCCCTGGTTTCTCTTC)	This Paper	N/A

(Continued on next page)

Continued

REAGENT or RESOURCE	SOURCE	IDENTIFIER
Primers for Mouse Il-6 (Forward: CAAAGCCAGAGTCCTTCAGAG; Reverse: GTCCTTAGCCACTCCTTCTG)	This Paper	N/A
Software and algorithms		
GraphPad Prism 8	GraphPad	N/A
MultiPoint Tool (Cell Counter)	ImageJ	N/A

RESOURCE AVAILABILITY

Lead contact

Further information and requests for resources and reagents should be directed to and will be fulfilled by the lead contact, Vaithilinaraja Arumugaswami (varumugaswami@mednet.ucla.edu).

Materials availability

This study did not generate new unique reagents.

Data and code availability

- RNA-seq data have been deposited at GEO and are publicly available as of the date of publication. Accession numbers are listed in the [key resources table](#). Microscopy data reported in this paper will be shared by the [lead contact](#) upon request.
- This study did not generate new original code.
- Any additional information required to reanalyze the data reported in this paper is available from the [lead contact](#) upon request.

EXPERIMENTAL MODEL AND SUBJECT DETAILS

Ethics statement

This study was performed in strict accordance with the recommendations of UCLA. All WNV, CHIKV and SARS-CoV-2 live virus experiments were performed at the UCLA BSL3 High containment facility.

Cells

HFF-1 (SCRC-1041) and Vero E6 [VERO C1008 (CRL-1586)] cells were obtained from ATCC. HFF-1 and Vero E6 cells were cultured in Dulbecco's Modified Eagle's Medium (DMEM) (Gibco) and Eagle's Minimum Essential Medium (EMEM) (Corning), respectively. DMEM contained 15% fetal bovine serum (FBS) and penicillin (100 units/mL), whereas EMEM growth media contained 15% FBS and penicillin (100 units/mL). Adenocarcinomic human alveolar basal epithelial A549 (CCL-185) cells from ATCC were cultured in the F12K (ATCC) media with the presence of 10% FBS and penicillin (100 units/mL). Cells were incubated at 37°C with 5% CO₂. Human pluripotent stem cell-derived cardiomyocytes (hPSC-CM) were provided by UCLA Cardiomyocyte Core and were derived as described below. The PSC-CMs were differentiated from hESC line H9 using a previously described method.⁷⁶ The hPSCs were maintained in mTeSR1 (STEMCELL Technology) and RPMI1640 [supplemented with B27 minus insulin (Invitrogen)] was used as differentiation medium. From Days 0–1, 6 μM CHIR99021 was added into differentiation medium. On Days 3–5, 5 μM IWR1 (Sigma-Aldrich) was added to the differentiation medium. Thereafter, on Day 7, RPMI 1640 plus B27 maintenance medium was added. Finally, on Days 10–11, RPMI 1640 without D-glucose and supplemented with B27 was transiently used for metabolic purification of CMs.³⁸

Viruses

CHIKV, WNV, ZIKV, EV-D68, RSV, SARS-Related Coronavirus 2 (SARS-CoV-2, Isolate USA-WA1/2020), were obtained from BEI Resources of National Institute of Allergy and Infectious Diseases (NIAID) or ATCC ([key resources table](#)). CHIKV, WNV, and SARS-CoV-2 were passaged once in Vero E6 cells and sequence verified viral stocks were aliquoted and stored at –80°C. Virus titer was measured in Vero E6 cells by established TCID50 assay.

In vivo mice experiment for CHIKV infection

C57BL/6J mice were used for infection study. Mice were housed at UCLA Vivarium. 14-month-old mixed sex mice (n = 5–6) were prophylactically (one day before CHIKV infection) or therapeutically (6h or 12h after CHIKV infection) treated with cAIMP (10 mg/kg) by intraperitoneal injection. The control group (n = 5) received only saline injection. The mice were inoculated with CHIKV (strain 18½5; 1 × 10⁵ pfu per mouse in a 20 μL volume) in the left rear footpad by subcutaneous injection. The animals

were observed for the next 7–59 days for clinical signs of footpad swelling. The footpad volume was measured using caliper and mice were humanely euthanized for tissue collection for histopathological analysis. Illumina reads from all animal rear left footpad RNA samples (7 dpi) were mapped to mouse (mm39) reference genome using STAR 2.7.9a⁷⁷ and subsequently the read counts per gene were quantified. The differential gene expression analysis was performed using DESeq2 v1.28.1 in R v4.0.3.⁷⁸ Genes that expressed differentially were considered only if they were supported by a false discovery rate FDR <0.05. Reactome pathway analysis was performed for DEGs using *Mus musculus* all genes as reference dataset in the Reactome v65⁷⁹ implemented in PANTHER. The overrepresented pathways in up or downregulated gene sets were only considered if they were supported by FDR <0.05.

METHOD DETAILS

Drug library and compounds

The compounds tested were obtained from InvivoGen, Millipore Sigma and Selleckchem (Table S4). A selected library of PAMP molecules was procured from InvivoGen since this library contains inhibitors for many key PRRs. All compounds were provided lyophilized and reconstituted in Nuclease-Free water (Invitrogen) or DMSO at the recommended solubility by manufacturer. Lyophilized and reconstituted compounds were aliquoted and stored at –20°C. Repeated freeze-thaw cycles were avoided whenever possible.

Viral infection for drug testing

HFF-1 cells were seeded at 1×10^4 cells per well in 0.2 mL volumes using a 96-well plate. Cells were treated with indicated compounds. 24 h later, viral inoculum of CHIKV (MOI of 0.1; 100 μ L/well), WNV (MOI of 1; 100 μ L/well), or ZIKV (MOI of 0.1; 100 μ L/well), was added onto HFF-1 cells using serum-free base media. The hPSC-CMs were plated at 1×10^5 cells per well in a 48-well plate. For hPSC-CMs, in addition to the previously-mentioned viruses, 100 μ L of prepared inoculum of EV-D68 (MOI of 0.1; 100 μ L/well), RSV (MOI of 0.1; 100 μ L/well), or SARS-CoV-2 (MOI of 0.01; 100 μ L/well) was added onto cells after removing the conditioned media from each well. After 1 h incubation at 37°C with 5% CO₂, inoculum was replaced with RPMI 1640 + B27 supplement with insulin. Cells were then fixed at selected timepoints with 4% PFA, collected by 1xRIPA for protein analysis, and/or supernatant collected for viral titer. Viral infection was examined by immunostaining using viral antigen-specific antibodies (key resources table). The captured immunostained images were used for quantification of the positively infected cells using ImageJ's Multipoint and Cell Counter feature. Based on the number of infected cells, the percent inhibition was calculated for each compound at its indicated dose. Subsequently, the IC50 values were calculated by fitting the data in a sigmoidal curve for an eight-dose response. Western Blot was subsequently used to confirm viral antigen expression.

Viral titer by TCID50 (median tissue culture infectious dose) assay

The method used to measure viral production by infected cells was accomplished by quantifying TCID50 as previously described.⁸⁰ Briefly, Vero E6 cells (density of 5×10^3 cells/well) were plated in 96-well plates. The next day, culture media samples collected from cardiomyocytes at various timepoints were subjected to 10-fold serial dilutions (10^1 to 10^8) and added onto Vero E6 cells. The cells were incubated at 37°C with 5% CO₂. Then 3 to 4 days after, each inoculated well was carefully evaluated for presence or absence of viral CPE. Thereafter, the percent infected dilutions immediately above and immediately below 50% were determined. TCID50 was calculated based on the method of Reed and Muench.

Cell viability and ATP assay

We performed Cell-Titer Glo Luminescent Assay (Promega) as indicated by manufacturer for assessing viability and intracellular ATP level. HFF-1 cells were seeded on 96-well plates. After 48 h of drug treatment, a working reagent (100 μ L) was added to the cells and incubated for 30 min at room temperature. Thereafter, 100 μ L of the cell-reagent reaction was transferred to a 96-well white bottom plate. The luminescence of each condition was measured in triplicate values and recorded. Percent viability for each compound was calculated based on vehicle (water or DMSO) treated cells.

NAD/NADH-Glo assay

We performed NAD/NADH Glo Luminescent Assay (Promega) as indicated by manufacturer for measuring intracellular NADH level. HFF-1 cells were seeded on 96-well plates and subjected to drug treatment and CHIKV infection. After 48 hpi, a working reagent (50 μ L) was added to the cells (50 μ L media volume) and incubated for 45 min at room temperature. The luminescence signal of 100 μ L of the cell-reagent reaction was quantified in triplicate values and analyzed.

Histopathology

Histopathological services were provided by UCLA Translational Pathology Core Lab. Mice footpad samples were processed, decalcified and sectioned for H&E staining, and subsequent image analysis. Immunohistochemistry stainings were also performed on these footpad tissues: Paraffin-embedded sections were cut at 4- μ m thickness and paraffin was removed with xylene and the sections were rehydrated through graded ethanol. Endogenous peroxidase activity was blocked with 3% hydrogen peroxide in methanol for 10 min. Heat-induced antigen retrieval was carried out for all sections in AR9 buffer (AR9001KT Akoya) using a Biocare decloaker at 95°C for 25 min. The slides were then stained with primary antibodies targeting mouse F4/80, CD4 and CD8 antigens at 4°C

overnight; the signal was detected using Bond Polymer Refine Detection Kit (Leica Microsystems, catalog #DS9800) with a diaminobenzidine reaction to detect antibody labeling and hematoxylin counterstaining.

Immunohistochemistry

Cells were fixed with methanol (incubated in -20°C freezer until washed with PBS) or 4% paraformaldehyde for 30–60 min. Cells were washed 3 times with 1x PBS and permeabilized using blocking buffer (0.3% Triton X-100, 2% BSA, 5% Goat Serum, 5% Donkey Serum in 1 X PBS) for 1 h at room temperature. For immunostaining, cells were incubated overnight at 4°C with each primary antibody. The cells were then washed with 1X PBS three times and incubated with respective secondary antibody for 1 h at room temperature. Nuclei were stained with DAPI (4',6-Diamidino-2-Phenylindole, Dihydrochloride) (Life Technologies) at a dilution of 1:5000 in 1X PBS. Image acquisition was done using Leica DM IRB fluorescent microscopes.

Viral infection and RNA sample preparation for RNA sequencing analysis

To determine cellular response to drug treatment and CHIKV infection, the HFF-1 cells in 12-well plate format were subjected to either vehicle or drug (cAIMP or Scleroglucan at $100\ \mu\text{g}/\text{mL}$) pretreatment. The next day, cells were inoculated with individual CHIKV, WNV or ZIKV (MOI of 0.1) and after 1 h of incubation for viral adsorption, the inoculum were replaced with complete DMEM media. We included mock-infected but vehicle-treated cells as negative control. We used quadruplicate wells for each condition. 24hpi, the cells were lysed with 1 mL of Trizol and proceeded with total RNA isolation as described below. The bulk RNA was extracted using RNeasy Mini Kit (Qiagen), as per the manufacturer's instructions. RNA was quantified using a NanoDrop 1,000 Spectrophotometer (Thermo Fisher Scientific). Duplicate RNA samples per treatment condition were submitted to the UCLA Technology Center for Genomics & Bioinformatics (TCGB) for RNA sequencing analysis.

RNA sequencing data analysis

Libraries for RNA-Seq that were prepared with KAPA Stranded mRNA-Seq Kit. The workflow consists of mRNA enrichment and fragmentation, first strand cDNA synthesis using random priming followed by second strand synthesis converting cDNA:RNA hybrid to double-stranded cDNA (dscDNA), and incorporates dUTP into the second cDNA strand. cDNA generation is followed by end repair to generate blunt ends, A-tailing, adaptor ligation and PCR amplification. Different adaptors were used for multiplexing samples in one lane. Sequencing was performed on Illumina NovaSeq 6000 for PE 2 \times 50 run. Data quality check was done on Illumina SAV. Demultiplexing was performed with Illumina Bcl2fastq v2.19.1.403 software. Partek Flow⁸¹ as used for all data analysis. Illumina reads from all HFF-1 samples were mapped to human (GRCh38) reference genome using STAR 2.7.9a⁷⁷ and subsequently the read counts per gene were quantified. For CHIKV data, the reads were mapped to combined human (GRCh38) and Chikungunya virus (NC_004162.2) reference genome to additionally quantify the read counts per CHIKV genes. The differential gene expression analysis was performed using DESeq2 v1.28.1 in R v4.0.3⁷⁸ Median of ratios method was used to normalize expression counts for each gene in all samples studied. Each gene in the samples was fitted into a negative binomial generalized linear model. Genes that expressed differentially were considered only if they were supported by a false discovery rate (FDR) $p < 0.01$ and Log2 Fold Change (FC) more than 1 and -1 for up- and down-regulated genes, respectively. Unsupervised principal component analysis (PCA) was performed using DESeq2 in R v4.1.1. The gene ontology (GO) enrichment overrepresentation test was performed in PANTHER v16.0⁸² using PANTHER GO-SLIM Biological Process annotation dataset.⁸³ Reactome pathway analysis was also performed for DEGs using human all genes as reference dataset in the Reactome v65⁷⁹ implemented in PANTHER. GO and Reactome pathway were only considered if they were supported by FDR $p < 0.05$. The ggplot2 v3.3.5 in R and Prism GraphPad v8.4.3 were used to generate figures. The heatmaps were generated using pheatmap v1.0.12 in R. RNA-seq data were deposited to the NCBI GEO under the accession number GSE197744.

Western blot analysis

For protein analysis, cells were lysed in 50 mM Tris pH 7.4, 1% NP-40, 0.25% sodium deoxycholate, 1 mM EDTA, 150 mM NaCl, 1 mM Na_3VO_4 , 20 mM or NaF, 1mM PMSF, 2 mg mL^{-1} aprotinin, 2 mg mL^{-1} leupeptin and 0.7 mg mL^{-1} pepstatin or Laemmli Sample Buffer (Bio Rad, Hercules, CA). Cell lysates were resolved by SDS-PAGE using 10% gradient gels (Bio-Rad) and transferred to a $0.2\ \mu\text{m}$ PVDF membrane (Bio-Rad). After the transfer, the membranes were blocked (5% skim milk and 0.1% Tween 20) in 1x TBST (0.1% Tween 20) at room temperature (RT) for 1 h. The membranes were then incubated with respective monoclonal antibodies overnight at 4°C and detected by Super-Signal West Femto Maximum Sensitivity Substrate (Thermo Scientific). Membranes were visualized with Bio-Rad ChemiDoc MP Imaging System.

QUANTIFICATION AND STATISTICAL ANALYSIS

Image analysis/quantification

Microscope images were obtained using the Leica DM IL LED Fluo and Leica LAS X Software Program. Then, 4–8 images per well were taken and quantified for each condition and timepoint using ImageJ's plugin Multipoint and Cell Counter feature to count the positively-stained cells by a double blinded approach.

Statistics and data analysis

Using GraphPad Prism, version 8.1.2, IC50 values were obtained by fitting a sigmoidal curve onto the data of an eight-point dose-response curve experiment. In addition, data was analyzed for statistical significance using unpaired Student's *t* test to compare two groups (uninfected vs. infected) or a non-parametric t-test (Mann-Whitney Test) with GraphPad Prism software, also version 8.1.2 (GraphPad Software, US). All statistical testing was performed at the two-sided alpha level of 0.05.